A MIXTURE FLUX APPROACH FOR ACCURATE AND ROBUST RESOLUTION OF TWO-PHASE FLOWS

TORE FLATTEN[A] AND STEINAR EVJE[B,C]

Abstract. The aim of this paper is to construct robust and accurate hybrid FVS/FDS type of schemes for a standard four-equation isentropic compressible two-fluid model governing 1-dimensional flow of a gas (g) and liquid (l) mixture. The starting point for our investigations is a Roe scheme and a hybrid FVS/FDS scheme. The latter is an AUSMD type of scheme obtained through a natural and rather straightforward extension of the corresponding scheme for the Euler equations (single-phase model) as described by Wada and Liou (1997, SIAM J. Sci. Comput. 18, 633–657). The main advantage of such hybrid FVS/FDS schemes is that they neither require the use of Riemann solvers nor the computation of nonlinear flux Jacobians. However, we observe that the two-phase AUSMD scheme is prone to introducing oscillations and overshoots around discontinuities. Based on the belief that this deficiency is due to the loose coupling between mass and momentum equations in the discretization of the two-phase model, we propose a method for improving the approximation properties of hybrid FVS/FDS schemes by enforcing a tighter coupling between the various equations.

The method, which is denoted as a "Mixture Flux" (MF) method, is composed of two main ingredients. First, we make use of an additional pressure evolution equation which is derived from the equation describing the conservation of the total mass. This provides us with information how to construct an appropriate numerical flux for the discretization of the pressure term of the momentum equations. Second, we introduce a consistent decomposition of the numerical mass fluxes into two components; one flux component F^{D} associated with the fast-moving pressure waves and another component F^{A} associated with the slow-moving volume fraction waves. The F^{D}-component is designed by using information from the momentum equations and is crucial for ensuring non-oscillatory behavior around the slow-moving volume fraction waves, whereas the F^{A}-component is responsible for the accuracy of these waves.

Particularly, by associating the flux F^{A} with the AUSMD mass flux we demonstrate through numerical experiments that the resulting MF-AUSMD scheme possesses accuracy and stability properties on the same level as the Roe scheme while allowing for highly improved computational efficiency. In addition, by using a slight modification of MF-AUSMD we can also simulate flow cases which locally involve transition from two-phase to single-phase.

The MF-method represents a general strategy for refining hybrid FVS/FDS schemes for two-phase flow models.

subject classification. 76T10, 76N10, 65M12, 35L65

key words. two-phase flow, two-fluid model, hyperbolic system of conservation laws, flux splitting, explicit scheme

1. Introduction

Among several two-phase flow models there are two fundamentally different formulations of the macroscopic field equations for the two-phase flow system; namely the *two-fluid* model and the *mixture* model [24], which is a simplified isothermal two-phase model consisting of separate mass conservation equations and a mixture momentum equation. Here we focus on the two-fluid model, which is considered to give a more general and detailed description of transient two-phase flows.

Date: July 21, 2003.

[A]Department of Energy and Process Engineering, Norwegian University of Science and Technology, Kolbjørn Hejes vei 1B, N-7491, Trondheim, Norway.

[B]RF-Rogaland Research, Thormøhlensgt. 55, N–5008 Bergen, Norway.

Email: steinar.evje@rf.no, tore.flatten@maskin.ntnu.no.

[C]Corresponding author.

This model is expressed as a set of 4 partial differential equations, one mass and one momentum conservation equation for each phase. The interaction terms between the two phases appear in the basic equations as transfer terms across the interfaces (source terms). More precisely, the basic form of the model can be written on the following vector form:

$$\partial_t \begin{pmatrix} \rho_{\rm g}\alpha_{\rm g} \\ \rho_{\rm l}\alpha_{\rm l} \\ \rho_{\rm g}\alpha_{\rm g}v_{\rm g} \\ \rho_{\rm l}\alpha_{\rm l}v_{\rm l} \end{pmatrix} + \partial_x \begin{pmatrix} \rho_{\rm g}\alpha_{\rm g}v_{\rm g} \\ \rho_{\rm l}\alpha_{\rm l}v_{\rm l} \\ \rho_{\rm g}\alpha_{\rm g}v_{\rm g}^2 + \alpha_{\rm g}p \\ \rho_{\rm l}\alpha_{\rm l}v_{\rm l}^2 + \alpha_{\rm l}p \end{pmatrix} = \begin{pmatrix} 0 \\ 0 \\ p\partial_x\alpha_{\rm g} + \tau_{\rm g} \\ p\partial_x\alpha_{\rm l} + \tau_{\rm l} \end{pmatrix} + \begin{pmatrix} 0 \\ 0 \\ Q_{\rm g} + M_{\rm g}^{\rm D} \\ Q_{\rm l} + M_{\rm l}^{\rm D} \end{pmatrix}. \tag{1}$$

Here α_k is the volume fraction of phase k with $\alpha_{\rm l} + \alpha_{\rm g} = 1$, ρ_k and v_k denote the density and fluid velocities of phase k, and p is the pressure common to both phases. Moreover, τ_k represents the interfacial forces which contain differential terms (hence, is relevant for the hyperbolicity of the model) and satisfy $\tau_{\rm g} + \tau_{\rm l} = 0$. $M_k^{\rm D}$ represents interfacial drag force with $M_{\rm g}^{\rm D} + M_{\rm l}^{\rm D} = 0$ whereas Q_k represent source terms due to gravity, friction, etc.

During the last decade, flux-splitting techniques denoted as "Advection Upstream Splitting Methods" (AUSM) have become popular for solving the equations of gas dynamics [13, 12, 30, 5]. An advantage of such methods is that they do not require a knowledge of the full eigenstructure of the system, and are consequently more efficient than classical approximate Riemann solvers like the Godunov [16, 11] and Roe [19, 20] schemes.

A recent trend has been to adapt such ideas to two-phase flow models [6, 14, 15]. Evje and Fjelde [7, 8] considered the mixture two-phase model. Basically, it was found that an AUSM scheme based on a rough estimate of the sound velocity gave accurate and non-oscillatory resolution of mass fronts comparable with the more computationally demanding Roe scheme [21, 10].

Regarding the two-fluid model, Paillère et al [17] investigated an extension of the AUSM$^+$ scheme of Liou [12] on a model including an energy conservation equation for each phase. Evje and Flatten [9] investigated a related approach, using an extension of the AUSMD/V scheme of Wada and Liou [30] on the two-fluid model. Results similar to the work of Paillère et al were obtained.

A feature common to both these approaches is a tendency towards introducing spurious oscillations and overshoots around discontinuities. Based on the belief that this deficiency is due to the loose coupling between mass and momentum equations in the discretization procedure, we here propose a general method for improving the approximation properties of such hybrid FVS/FDS schemes for the two-phase model. The main idea behind this novel construction can be described as follows: Assuming that the phases have equal pressure, the mass coupling can be expressed as (writing $m_k = \rho_k\alpha_k$)

$$\frac{m_{\rm g}}{\rho_{\rm g}(p)} + \frac{m_{\rm l}}{\rho_{\rm l}(p)} = 1, \tag{2}$$

which is a rewritten form of the basic volume fraction equation

$$\alpha_{\rm g} + \alpha_{\rm l} = 1.$$

The relation (2) contains essential information about the interrelation between the masses and the pressure. The idea of this work is to derive hybrid FVS/FDS schemes which explicitly make use of this relation in the construction of appropriate numerical mass fluxes. Basically, the implementation of this idea is carried out in two steps.

- First, we couple the pressure calculation more directly to the momentum equations. For this purpose, we derive a pressure evolution equation by combining the mass conservation equations (two first equations of (1)) and the relation (2). This pressure equation is discretized at the cell interface whereas cell-centered pressure values are obtained directly from (2). We apply a discretization of the pressure evolution equation which enforces a coupling between the cell interface pressure $p_{j+1/2}$ and cell-centered pressure p_j, ensuring consistency of the pressure splitting.
- Second, we couple the calculation of masses m_k closer to the momentum equations. To achieve this, we employ (2) and derive consistent numerical mass fluxes associated with the mass conservation equations which are composed of two components; one diffusive part $F^{\rm D}$

for stable (non-oscillatory) resolution of volume fraction waves and another nondissipative part F^{A} for accurate resolution of these waves.

The above two steps bring forth numerical fluxes for the various equations of (1) which consist of a *mixture* of terms from the other equations. This motivates us to denote the general algorithm as a *Mixture Flux* (MF) method. Consequently, we lose some of the simplicity of the original AUSM concept which basically treats the system as a set of scalar equations without accounting for the interrelation between the various equations. However, the efficiency properties of the original AUSM type schemes largely remain for the proposed MF-type schemes as we still avoid use of Riemann solvers and computation of nonlinear flux Jacobians.

Particularly, by associating the flux component F^{A} with the AUSMD flux used in [9] we obtain a MF-AUSMD scheme. We formally demonstrate that under natural assumptions on the F^{D} flux component, the resulting MF-AUSMD scheme recovers the numerical flux of an exact Riemann solver for a moving or stationary contact discontinuity. This ensures that mass fronts are properly resolved. We also verify that Abgrall's principle [1] is satisfied; that a flow, uniform in velocity and pressure, must remain uniform during its temporal evolution.

We demonstrate through numerical experiments that the proposed MF-AUSMD scheme matches the good accuracy and stability properties of the Roe scheme. More precisely, the MF-AUSMD is slightly more diffusive on the fast moving sonic waves. For the approximation of the slow volume fraction waves we see that the MF-AUSMD scheme and the Roe scheme behave very similar. In particular, the deficiencies of the AUSMD scheme studied in [9] have been removed. In addition, we may easily modify the MF-AUSMD scheme so that it can handle flow cases which locally involve transition from two-phase to single-phase flow.

Hence, the MF-AUSMD scheme, which is totally free from Riemann solvers and computation of nonlinear flux Jacobians, allows for highly improved computational efficiency compared to the Roe scheme.

Our paper is organized as follows: In Section 2 we present the two-fluid model we will be working with. In section 3 we briefly restate the flux-splitting schemes that were investigated in [9] and which will be used as a basis for the methods we develop in this paper. The purpose of Section 4 is to motivate for the Mixture Flux method by observing some "weak points" of the flux-splitting schemes considered in [9]. In Section 5 we introduce the Mixture Flux method, and in Section 6 we verify that the method satisfies certain "good" properties. In Section 7 we apply it to a set of test cases found in the literature. Comparisons are made with the Roe scheme as well as the AUSMD scheme considered in [9] and an appropriate modification is applied making the scheme able to handle the transition to one-phase flow.

2. The Two-Fluid Model

Throughout this paper we will be concerned with the common two-fluid model formulated by stating separate conservation equations for mass and momentum for the two fluids, which we will denote as a gas (g) and a liquid (l) phase. The model has been studied by several authors [28, 3, 4, 17, 9] and will be briefly stated here. We let $\mathbf{U}$ be the vector of conserved variables

$$\mathbf{U} = \begin{bmatrix} \rho_{\mathrm{g}}\alpha_{\mathrm{g}} \\ \rho_{\mathrm{l}}\alpha_{\mathrm{l}} \\ \rho_{\mathrm{g}}\alpha_{\mathrm{g}}v_{\mathrm{g}} \\ \rho_{\mathrm{l}}\alpha_{\mathrm{l}}v_{\mathrm{l}} \end{bmatrix} = \begin{bmatrix} m_{\mathrm{g}} \\ m_{\mathrm{l}} \\ I_{\mathrm{g}} \\ I_{\mathrm{l}} \end{bmatrix}. \tag{3}$$

By using the notation $\Delta p = p - p^{\mathrm{i}}$, where p^{i} is the interfacial pressure, and $\tau_k = (p^{\mathrm{i}} - p)\partial_x\alpha_k = -\Delta p\partial_x\alpha_k$, we see that the model (1) can be written on the form

- Conservation of mass

$$\frac{\partial}{\partial t}\left(\rho_{\mathrm{g}}\alpha_{\mathrm{g}}\right) + \frac{\partial}{\partial x}\left(\rho_{\mathrm{g}}\alpha_{\mathrm{g}}v_{\mathrm{g}}\right) = 0, \tag{4}$$

$$\frac{\partial}{\partial t}\left(\rho_{\mathrm{l}}\alpha_{\mathrm{l}}\right) + \frac{\partial}{\partial x}\left(\rho_{\mathrm{l}}\alpha_{\mathrm{l}}v_{\mathrm{l}}\right) = 0, \tag{5}$$

- Conservation of momentum

$$\frac{\partial}{\partial t}\left(\rho_{\mathrm{g}}\alpha_{\mathrm{g}}v_{\mathrm{g}}\right)+\frac{\partial}{\partial x}\left(\rho_{\mathrm{g}}\alpha_{\mathrm{g}}v_{\mathrm{g}}^2+\alpha_{\mathrm{g}}\Delta p\right)+\alpha_{\mathrm{g}}\frac{\partial}{\partial x}(p-\Delta p)=Q_{\mathrm{g}}+M_{\mathrm{g}}^{\mathrm{D}}, \tag{6}$$

$$\frac{\partial}{\partial t}\left(\rho_{\mathrm{l}}\alpha_{\mathrm{l}}v_{\mathrm{l}}\right)+\frac{\partial}{\partial x}\left(\rho_{\mathrm{l}}\alpha_{\mathrm{l}}v_{\mathrm{l}}^2+\alpha_{\mathrm{l}}\Delta p\right)+\alpha_{\mathrm{l}}\frac{\partial}{\partial x}(p-\Delta p)=Q_{\mathrm{l}}+M_{\mathrm{l}}^{\mathrm{D}}. \tag{7}$$

Since we focus on the development of numerical schemes which can handle the basic two-fluid model, we have set the interfacial drag force terms to zero, i.e. $M_{\mathrm{g}}^{\mathrm{D}}=M_{\mathrm{l}}^{\mathrm{D}}=0$.

In addition, other constitutive laws are needed to close the system. In particular, the volume fractions must satisfy

$$\alpha_{\mathrm{g}}+\alpha_{\mathrm{l}}=1. \tag{8}$$

The system is closed by some equation of states (EOS) for the liquid and gas phase. The numerical methods we study in this work allow general expressions for the EOS. However, for the numerical simulations presented in this work we assume the simplified thermodynamic relations

$$\rho_{\mathrm{l}}=\rho_{\mathrm{l},0}+\frac{p-p_0}{a_{\mathrm{l}}^2} \tag{9}$$

and

$$\rho_{\mathrm{g}}=\frac{p}{a_{\mathrm{g}}^2} \tag{10}$$

where

$$\begin{aligned} p_0&=1\text{ bar}=10^5\text{ Pa}\\ \rho_{\mathrm{l},0}&=1000\text{ kg/m}^3,\\ a_{\mathrm{g}}^2&=10^5(\text{m/s})^2\\ a_{\mathrm{l}}&=10^3\text{ m/s}. \end{aligned}$$

The models (9) and (10) correspond to a general stiffened gas EOS of the form

$$p=(\gamma_k-1)a_k^2\rho_k-\gamma_k\pi_k,$$

where $\pi_k=(a_k^2\rho_{k,0}-p_0)/2$ where $\rho_{k,0}$ represents the material density and p_0 the ambient pressure. γ_k and π_k are constants specific for each phase. Particularly, by choosing $\gamma_{\mathrm{l}}=2$ we recover (9) while (10) is obtained by choosing $\gamma_{\mathrm{g}}=2$ and $\pi_{\mathrm{g}}=0$.

Moreover, we will treat Q_k as a pure source term, assuming that it does not contain any differential operators. We use the interface pressure correction

$$\Delta p=\sigma\frac{\alpha_{\mathrm{g}}\alpha_{\mathrm{l}}\rho_{\mathrm{g}}\rho_{\mathrm{l}}}{\rho_{\mathrm{g}}\alpha_{\mathrm{l}}+\rho_{\mathrm{l}}\alpha_{\mathrm{g}}}(v_{\mathrm{g}}-v_{\mathrm{l}})^2, \tag{11}$$

where we set $\sigma=1.2$. This choice ensures that the model is a hyperbolic system of conservation laws, see for instance [4, 9]. Another feature of this model is that it possesses an approximate mixture sound velocity c given by

$$c=\sqrt{\frac{\rho_{\mathrm{l}}\alpha_{\mathrm{g}}+\rho_{\mathrm{g}}\alpha_{\mathrm{l}}}{\frac{\partial\rho_{\mathrm{g}}}{\partial p}\rho_{\mathrm{l}}\alpha_{\mathrm{g}}+\frac{\partial\rho_{\mathrm{l}}}{\partial p}\rho_{\mathrm{g}}\alpha_{\mathrm{l}}}}. \tag{12}$$

We refer to [28, 9] for more details.

Having solved for the conservative variable $\mathbf{U}$, we need to obtain the primitive variables $(\alpha_{\mathrm{g}},p,v_{\mathrm{g}},v_{\mathrm{l}})$. For the pressure variable we see that by writing the volume fraction equation (8) in terms of the conserved variables as

$$\frac{m_{\mathrm{g}}}{\rho_{\mathrm{g}}(p)}+\frac{m_{\mathrm{l}}}{\rho_{\mathrm{l}}(p)}=1, \tag{13}$$

we obtain a relation yielding the pressure $p(m_{\mathrm{g}},m_{\mathrm{l}})$. Using the relatively simple form of EOS given by (9) and (10) we see that the pressure p is found as a positive root of a second order polynomial. For more general EOS we must solve a non-linear system of equations, for instance by using a

Newton-Rapson algorithm. Moreover, the fluid velocities v_{g} and v_{l} are obtained directly from the relations

$$v_{\mathrm{g}} = \frac{U_3}{U_1}, \qquad v_{\mathrm{l}} = \frac{U_4}{U_2}.$$

Remark 1. *Throughout this work we will study only the isentropic 4-equation model given above. The inclusion of energy equations does not significantly alter the existing eigenstructure of the isentropic model, but adds entropy waves moving with the fluid velocities. It is our belief that the main difficulties related to the strong phasic couplings in the pressure and volume fraction waves are fully present in the isentropic model. Formally, the method investigated in this paper should be naturally extensible to the full model. This will be explored elsewhere.*

Remark 2. *Concerning the EOS for the liquid and gas phase, we emphasize that the methods we develop do not require simple linear relations as given by* (9) *and* (10)*. In principle, the only point which is affected by using more complicated EOS is the resolution algorithm which determines the pressure from the general relation* (13)*.*

Remark 3. *The Mixture Flux approach we propose in this paper is to a large extent independent of the hyperbolicity assumption since it does not rely on any Riemann solver nor calculation of flux jacobians. Thus, there are good reasons to believe that MF-schemes can be used to explore problems where the model becomes non-hyperbolic. More generally, since the dependence on the special properties of the underlying model is weak, the MF-methods should have a potential for becoming a useful tool when studying what happens when perturbation parameters reach critical values such that the nature of the model changes.*

3. Two Hybrid FVS/FDS Numerical Schemes

We here briefly restate two of the flux splitting schemes we investigated in [9], the van Leer scheme and the modified version denoted as AUSMD. Both are discrete schemes of the general form

$$\begin{aligned}\mathbf{U}_j^{n+1} = \mathbf{U}_j^n &- \frac{\Delta t}{\Delta x}\left(\mathbf{F}^c(\mathbf{U}_j^n, \mathbf{U}_{j+1}^n) - \mathbf{F}^c(\mathbf{U}_{j-1}^n, \mathbf{U}_j^n)\right)\\ &- \frac{\Delta t}{\Delta x}\left(\mathbf{F}^p(\mathbf{U}_j^n, \mathbf{U}_{j+1}^n) - \mathbf{F}^p(\mathbf{U}_{j-1}^n, \mathbf{U}_j^n)\right)\\ &- \frac{\Delta t}{\Delta x}\left(\mathbf{H}\frac{\partial p^{\mathrm{i}}}{\partial x}\right)_j + \Delta t \mathbf{Q}_j^n.\end{aligned}$$

Here $\mathbf{F}^c$ and $\mathbf{F}^p$ are numerical fluxes assumed to be consistent with the corresponding physical fluxes $\mathbf{f}^c$ and $\mathbf{f}^p$,

$$\mathbf{f}^c = \begin{pmatrix} \rho_{\mathrm{g}}\alpha_{\mathrm{g}}v_{\mathrm{g}} \\ \rho_{\mathrm{l}}\alpha_{\mathrm{l}}v_{\mathrm{l}} \\ \rho_{\mathrm{g}}\alpha_{\mathrm{g}}v_{\mathrm{g}}^2 \\ \rho_{\mathrm{l}}\alpha_{\mathrm{l}}v_{\mathrm{l}}^2 \end{pmatrix}, \qquad \mathbf{f}^p = \begin{pmatrix} 0 \\ 0 \\ \alpha_{\mathrm{g}}\Delta p \\ \alpha_{\mathrm{l}}\Delta p \end{pmatrix},$$

and $\mathbf{H}$ is given by

$$\mathbf{H} = \begin{pmatrix} 0 \\ 0 \\ \alpha_{\mathrm{g}} \\ \alpha_{\mathrm{l}} \end{pmatrix}.$$

We see that the fluxes of the the model (4)–(7) consist of three different sort of terms; convective flux terms $\partial_x(\rho\alpha v)$ and $\partial_x(\rho\alpha v^2)$, conservative pressure terms $\partial_x(\alpha\Delta p)$ and non-conservative pressure terms $\alpha\partial_x(p-\Delta p)$. The discretization of these terms follows closely the work of Wada and Liou [30] for Euler equations (except from the non-conservative pressure term which does not appear in their model).

3.1. Convective Flux Splitting for the $\mathbf{F}^c$-component.

3.1.1. *Van Leer.* We consider the velocity splitting formulas used in previous works [12, 30, 7, 8, 9].

$$V^{\pm}(v,c) = \begin{cases} \pm\frac{1}{4c}(v \pm c)^2 & \text{if } |v| \leq c \\ \frac{1}{2}(v \pm |v|) & \text{otherwise.} \end{cases}, \tag{14}$$

where the parameter c represents the physical sound velocity for the system. For the two-fluid model, we assume that it is given by the approximate expression (12). We now let the numerical fluxes be given as follows:

(1) *Mass Flux.* We let the numerical mass flux $(\rho\alpha v)_{j+1/2}$ be given as

$$(\rho\alpha v)_{j+1/2} = (\rho\alpha)_j V^+(v_j, c_{j+1/2}) + (\rho\alpha)_{j+1} V^-(v_{j+1}, c_{j+1/2}) \tag{15}$$

for each phase.

(2) *Momentum Flux.* We let the numerical convective momentum flux $(\rho\alpha v^2)_{j+1/2}$ be given as

$$(\rho\alpha v^2)_{j+1/2} = \frac{1}{2}(\rho\alpha v)_{j+1/2}(v_j + v_{j+1}) - \frac{1}{2}|(\rho\alpha v)_{j+1/2}|(v_{j+1} - v_j). \tag{16}$$

Here and in the following $c_{j+1/2} = \max(c_j, c_{j+1})$ in accordance with the practice of other works [30, 7, 9]. The van Leer scheme possesses good stability properties but is excessively diffusive, especially on the volume fraction waves. This motivates for proposing a mechanism for eliminating such numerical dissipation. This leads to the AUSMD scheme which we define next.

3.1.2. *AUSMD.* We consider the AUSMD scheme obtained by replacing the splitting formulas $V^{\pm}$ given by (14) and used in (15) and (16) with the less diffusive pair

$$\tilde{V}^{\pm}(v,c,\chi) = \begin{cases} \chi V^{\pm}(v,c) + (1-\chi)\frac{v \pm |v|}{2} & |v| < c \\ \frac{1}{2}(v \pm |v|) & \text{otherwise} \end{cases} \tag{17}$$

where

$$\chi_{\mathrm{L}} = \frac{2(\rho/\alpha)_{\mathrm{L}}}{(\rho/\alpha)_{\mathrm{L}} + (\rho/\alpha)_{\mathrm{R}}} \tag{18}$$

and

$$\chi_{\mathrm{R}} = \frac{2(\rho/\alpha)_{\mathrm{R}}}{(\rho/\alpha)_{\mathrm{L}} + (\rho/\alpha)_{\mathrm{R}}} \tag{19}$$

for each phase. In order to depict the main idea of the modification leading to AUSMD we consider a contact discontinuity given by

$$\begin{aligned} &p_{\mathrm{L}} = p_{\mathrm{R}} = p \\ &\alpha_{\mathrm{L}} \neq \alpha_{\mathrm{R}} \\ &(v_{\mathrm{g}})_{\mathrm{L}} = (v_{\mathrm{l}})_{\mathrm{L}} = (v_{\mathrm{g}})_{\mathrm{R}} = (v_{\mathrm{l}})_{\mathrm{R}} = v. \end{aligned} \tag{20}$$

All pressure terms vanish from the model (4)-(7), and it is seen that the solution to this initial value problem is simply that the discontinuity will propagate with a velocity corresponding to the velocity v. The exact solution of the Riemann problem will then give the numerical mass flux

$$(\rho\alpha v)_{j+1/2} = \frac{1}{2}\rho(\alpha_{\mathrm{L}} + \alpha_{\mathrm{R}})v - \frac{1}{2}\rho(\alpha_{\mathrm{R}} - \alpha_{\mathrm{L}})|v|. \tag{21}$$

It is easy to check that the use of the modified splitting functions (17)–(19) ensure that AUSMD mass fluxes satisfy (21) for the contact discontinuity (20). This is not true for the van Leer scheme.

3.2. **Pressure Splitting for the $\mathbf{F}^p$ and $\mathbf{F}^\alpha$-components.** The discretization of the pressure terms is the same for both schemes.

3.2.1. *Conservative pressure term.* We follow the approach used in [9] which is based on [30], where an upwind type of discretization was used. The conservative pressure term given by $\alpha\Delta p$ is discretized as follows

$$(\alpha\Delta p)_{j+1/2} = P^+(v_{\rm L}, c_{j+1/2})(\alpha\Delta p)_{\rm L} + P^-(v_{\rm R}, c_{j+1/2})(\alpha\Delta p)_{\rm R}. \tag{22}$$

where the pressure splitting formulas $P^{\pm}(v,c)$ are given by

$$P^{\pm}(v,c) = V^{\pm}(v,c)\cdot\begin{cases} \frac{1}{c}\left(\pm 2 - \frac{v}{c}\right) & \text{if } |v| \le c \\ \frac{1}{v} & \text{otherwise.} \end{cases} \tag{23}$$

3.2.2. *Non-conservative pressure term.* The non-conservative term is discretized as follows

$$\begin{aligned}\left(\alpha\frac{\partial p^i}{\partial x}\right)_j = \frac{1}{\Delta x}\Big(&\left[\bar\alpha_{j-1/2}P^+(v_j,\hat c_{j-1/2})p^i_j + \bar\alpha_{j+1/2}P^-(v_{j+1},\hat c_{j+1/2})p^i_{j+1}\right] \\ &- \left[\bar\alpha_{j-1/2}P^+(v_{j-1},\hat c_{j-1/2})p^i_{j-1} + \bar\alpha_{j+1/2}P^-(v_j,\hat c_{j+1/2})p^i_j\right]\Big),\end{aligned} \tag{24}$$

where

$$\bar\alpha_{j+1/2} = \frac{1}{2}(\alpha_j + \alpha_{j+1}).$$

We refer to [9] for a description of the motivation behind this particular discretization.

4. Some Observations

In the following two selected numerical examples taken from [9] will be presented. We want to compare the performance of the van Leer, AUSMD, and a Roe scheme and thereby reveal characteristic behavior. The implementation of the Roe scheme is described in [9].

As will be the case for all numerical simulations presented in this paper, our main concern will be to demonstrate the inherent accuracy and stability properties of the schemes. Consequently we limit ourselves to first order accuracy in space and time together with an explicit time integration.

4.1. **A Large Relative Velocity Shock.** We consider an initial Riemann problem also investigated by Cortes et al [4] for a similar two-fluid model. The initial states are given by

$$\mathbf{W}_{\rm L} = \begin{bmatrix} p \\ \alpha_{\rm l} \\ v_{\rm g} \\ v_{\rm l} \end{bmatrix} = \begin{bmatrix} 265000 \\ 0.71 \\ 65 \\ 1 \end{bmatrix} \tag{25}$$

and

$$\mathbf{W}_{\rm R} = \begin{bmatrix} p \\ \alpha_{\rm l} \\ v_{\rm g} \\ v_{\rm l} \end{bmatrix} = \begin{bmatrix} 265000 \\ 0.7 \\ 50 \\ 1 \end{bmatrix}. \tag{26}$$

No source terms are taken into account. We used the timestep $\Delta x/\Delta t = 10^3$ m/s and a computational grid of 100 cells. The results, plotted at the time $T = 0.1$ s, are given in Figure 1. The reference solution was computed using the Roe scheme on a fine grid of 10 000 cells. The existence of two separate volume fraction waves can be seen from the small wedge in liquid fraction at $x = 50$m. We make the following observations:

- The van Leer scheme is able to produce stable and nonoscillatory approximations, however, it is excessively diffusive on the slow volume fraction waves.
- The AUSMD produces a resolution of sonic waves which is comparable to that of the van Leer and Roe scheme. However, the slow volume fraction waves located around $x = 50$ m are reproduced with less numerical diffusion. Unfortunately numerical oscillations, which are especially severe for the liquid velocity, occur for AUSMD.

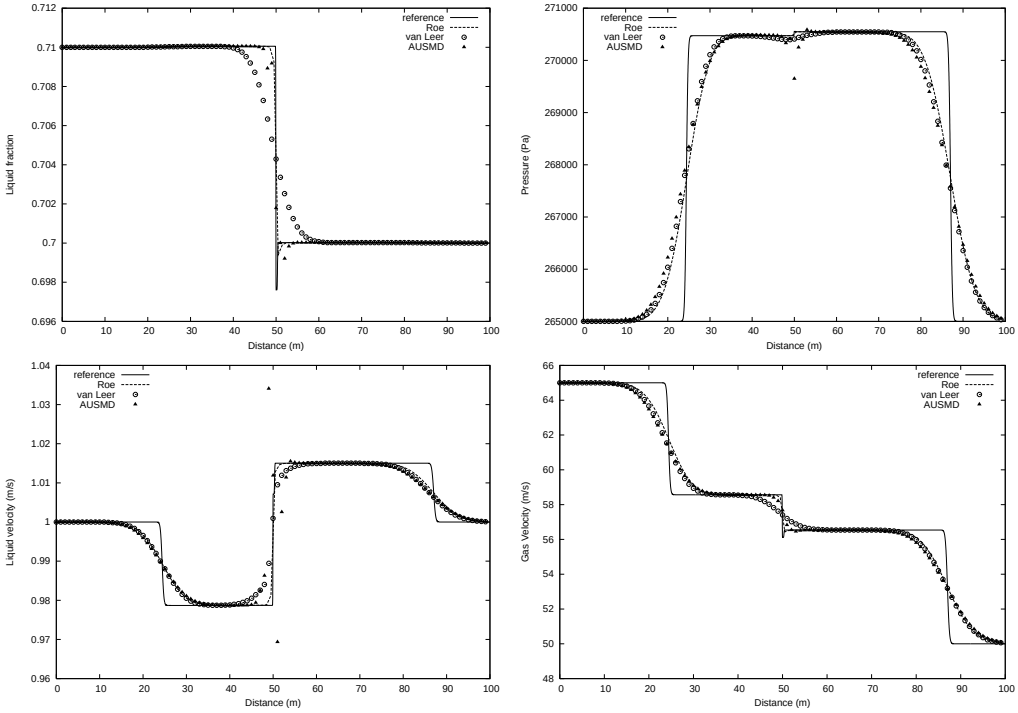

FIGURE 1. LRV shock tube problem. Comparison between van Leer, AUSMD, and Roe scheme on a grid of 100 cells. Top left: liquid fraction. Top right: pressure. Bottom left: liquid velocity. Bottom right: gas velocity.

4.2. **Water Faucet.** We now consider a benchmark faucet flow problem proposed by Ransom [18], which has been extensively studied [3, 9, 28, 15, 29, 17].

We consider a vertical pipe of length 12 m with the initial uniform state

$$\mathbf{W} = \begin{bmatrix} p \\ \alpha_{\mathrm{l}} \\ v_{\mathrm{g}} \\ v_{\mathrm{l}} \end{bmatrix} = \begin{bmatrix} 10^5 \text{ Pa} \\ 0.8 \\ 0 \\ 10 \text{ m/s} \end{bmatrix}. \tag{27}$$

Gravity is the only source term taken into account, i.e. in the framework of (6) and (7) we have

$$Q_k = g\rho_k\alpha_k, \tag{28}$$

with g being the acceleration of gravity. At the inlet we have the constant conditions $\alpha_{\mathrm{l}} = 0.8$, $v_{\mathrm{l}} = 10$ m/s and $v_{\mathrm{g}} = 0$. At the outlet the pipe is open to the ambient pressure $p = 10^5$ Pa. The remaining variables at the boundaries are determined by simple extrapolation.

A contact discontinuity in the volume fraction will arise as the liquid falls under the acceleration of gravity. It is possible to express an approximate solution in analytical form: [9, 29, 17]

$$v_{\mathrm{l}}(x,t) = \begin{cases} \sqrt{v_0^2 + 2gx} & \text{for } x < v_0 t + \frac{1}{2}gt^2 \\ v_0 + gt & \text{otherwise.} \end{cases} \tag{29}$$

$$\alpha_{\mathrm{l}}(x,t) = \begin{cases} \alpha_0(1 + 2gxv_0^{-2})^{-1/2} & \text{for } x < v_0 t + \frac{1}{2}gt^2 \\ \alpha_0 & \text{otherwise.} \end{cases} \tag{30}$$

The parameters $\alpha_0 = 0.8$ and $v_0 = 10$ m/s are the initial states.

A comparison between the AUSMD and the Roe scheme regarding the accuracy on volume fraction is given in Figure 2. For coarse grids, the AUSMD and Roe scheme produce similar solutions. However, AUSMD introduces a slight overshoot for 1200 cells, which increases in amplitude

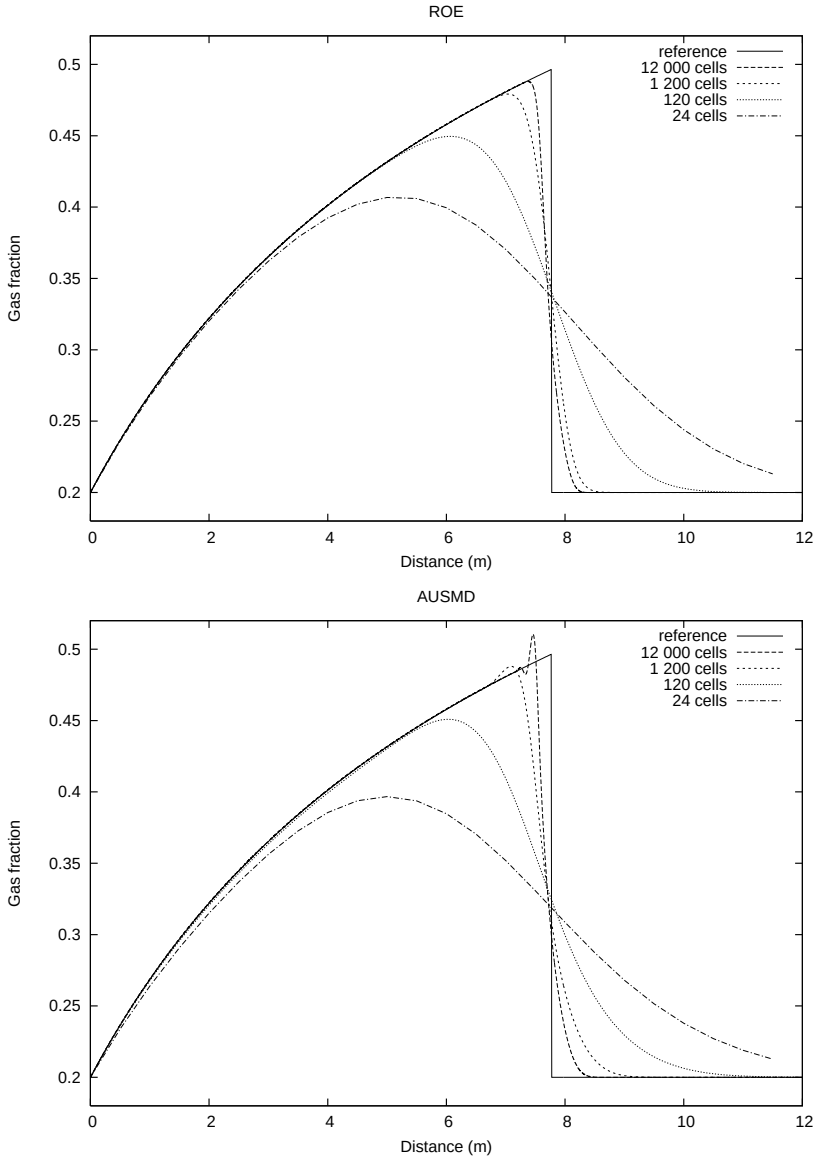

FIGURE 2. Water Faucet. t=0.6 s. Accuracy on volume fraction. Top: Grid refinement for Roe scheme. Bottom: Grid refinement for AUSMD scheme.

with further grid refinement. This contrasts the Roe scheme where the reference solution seems to be approached in a fully monotone way.

This problem indicates the same as we observed for the previous example: *AUSMD has some problems with resolving the slow-moving volume fraction waves without introducing oscillations.*

Remark 4. *Despite the above observed deficiency of the AUSMD scheme, the scheme still seems to be a good candidate for solving two-phase problems relevant e.g. for the petroleum industry. In* [9] *we demonstrated that by introducing a slight modification of the basic AUSMD scheme, mainly consisting of a switch to a more diffusive scheme like the van Leer scheme in the transition to single-phase flow, we could accurately solve difficult problems like separation of two phases and the oscillating manometer problem.*

4.3. **Conjecture.** The above numerical experiments indicate that the numerical fluxes of the Roe and the AUSMD scheme possess numerical dissipation of very similar strength. However, while

the Roe scheme gives stable and non-oscillatory approximations we observe that the AUSMD scheme tends to introduce oscillations and/or overshoot around volume fraction waves. We believe that this deficiency is due to the weak coupling between mass and momentum equations in the construction of numerical fluxes for AUSMD. Basically, the equations are discretized as a set of scalar equations. This strongly contrasts the Roe scheme which treats the model in a strongly coupled manner through the Jacobian matrix. In the next section, motivated by the success of the Roe scheme, we propose a general method for modifying hybrid FVS/FDS schemes such that the numerical flux associated with the pressure term as well as the numerical mass fluxes are composed of a mixture of components from the momentum equations and by that enforce a stronger coupling between the mass and momentum equations.

5. The Mixture Flux (MF) Method

The aim of this section is to develop a modification of the AUSMD scheme presented in Section 3 which possesses the following properties:

- Riemann-free solver;
- non-oscillatory approximations;
- accuracy comparable to the Roe scheme on all waves.

The starting point is the model (4)–(7) written on the form

$$\partial_t \begin{pmatrix} \rho_{\mathrm{g}}\alpha_{\mathrm{g}} \\ \rho_{\mathrm{l}}\alpha_{\mathrm{l}} \\ \rho_{\mathrm{g}}\alpha_{\mathrm{g}}v_{\mathrm{g}} \\ \rho_{\mathrm{l}}\alpha_{\mathrm{l}}v_{\mathrm{l}} \end{pmatrix} + \partial_x \begin{pmatrix} \rho_{\mathrm{g}}\alpha_{\mathrm{g}}v_{\mathrm{g}} \\ \rho_{\mathrm{l}}\alpha_{\mathrm{l}}v_{\mathrm{l}} \\ \rho_{\mathrm{g}}\alpha_{\mathrm{g}}v_{\mathrm{g}}^2 \\ \rho_{\mathrm{l}}\alpha_{\mathrm{l}}v_{\mathrm{l}}^2 \end{pmatrix} + \begin{pmatrix} 0 \\ 0 \\ \alpha_{\mathrm{g}}\partial_x p \\ \alpha_{\mathrm{l}}\partial_x p \end{pmatrix} + \begin{pmatrix} 0 \\ 0 \\ (\Delta p)\partial_x\alpha_{\mathrm{g}} \\ (\Delta p)\partial_x\alpha_{\mathrm{l}} \end{pmatrix} = \begin{pmatrix} 0 \\ 0 \\ Q_{\mathrm{g}} \\ Q_{\mathrm{l}} \end{pmatrix}. \tag{31}$$

As a motivation, before introducing the modified solution method we now focus on the following two observations:

5.1. Two Observations relevant for the MF method.

Observation 1. We have already observed that the pressure is related to the masses m_{g} and m_{l} through the static relation (13). In the following we want to demonstrate how the pressure is related to the momentums $\rho_k\alpha_k v_k$ through a certain dynamical relation.

To see this, we consider the total mass conservation equation obtained by adding the two separate mass conservation equations.

$$\frac{\partial}{\partial t}\left(m_{\mathrm{g}} + m_{\mathrm{l}}\right) + \frac{\partial}{\partial x}\left(\rho_{\mathrm{g}}\alpha_{\mathrm{g}}v_{\mathrm{g}} + \rho_{\mathrm{l}}\alpha_{\mathrm{l}}v_{\mathrm{l}}\right) = 0. \tag{32}$$

From (13) we have that

$$m_{\mathrm{g}} = m_{\mathrm{g}}(m_{\mathrm{l}}, p) = \left(1 - \frac{m_{\mathrm{l}}}{\rho_{\mathrm{l}}}\right)\rho_{\mathrm{g}}.$$

Consequently, we see that

$$\frac{\partial m_{\mathrm{g}}}{\partial m_{\mathrm{l}}} = -\frac{\rho_{\mathrm{g}}}{\rho_{\mathrm{l}}}, \qquad \frac{\partial m_{\mathrm{g}}}{\partial p} = \left[1 - \frac{m_{\mathrm{l}}}{\rho_{\mathrm{l}}}\right]\frac{\partial \rho_{\mathrm{g}}}{\partial p} + \left[\frac{m_{\mathrm{l}}\rho_{\mathrm{g}}}{\rho_{\mathrm{l}}^2}\right]\frac{\partial \rho_{\mathrm{l}}}{\partial p}. \tag{33}$$

Differentiating out the first temporal term of (32) and using (33) we get the following non-conservative differential equation for the pressure

$$\frac{\partial p}{\partial t} + \kappa\left(\rho_{\mathrm{l}}\frac{\partial}{\partial x}\left(\rho_{\mathrm{g}}\alpha_{\mathrm{g}}v_{\mathrm{g}}\right) + \rho_{\mathrm{g}}\frac{\partial}{\partial x}\left(\rho_{\mathrm{l}}\alpha_{\mathrm{l}}v_{\mathrm{l}}\right)\right) = 0 \tag{34}$$

where

$$\kappa = \frac{1}{\frac{\partial \rho_{\mathrm{l}}}{\partial p}\alpha_{\mathrm{l}}\rho_{\mathrm{g}} + \frac{\partial \rho_{\mathrm{g}}}{\partial p}\alpha_{\mathrm{g}}\rho_{\mathrm{l}}}. \tag{35}$$

Having seen that the pressure is directly related to the momentums $\rho_k\alpha_k v_k$, we also recall that the pressure p can be obtained from the masses $m_k = \rho_k\alpha_k$ through the relation (13). In the following we want to include *both* these aspects in the calculation of the pressure. First, as before we obtain the pressure p_j at the cell center from (13). In addition, we will introduce the pressure $p_{j+1/2}$ at

the cell interface, obtained through an appropriate discretization of the pressure evolution equation (34).

Observation 2. Again, noting that the relation (13) can be written on the form

$$m_{\mathrm{g}} = m_{\mathrm{g}}(m_{\mathrm{l}}, p) = \left(1 - \frac{m_{\mathrm{l}}}{\rho_{\mathrm{l}}(p)}\right)\rho_{\mathrm{g}}(p),$$

we see that

$$\begin{aligned} dm_{\mathrm{g}} &= (m_{\mathrm{g}})_{m_{\mathrm{l}}} dm_{\mathrm{l}} + (m_{\mathrm{g}})_p dp \\ &= -\frac{\rho_{\mathrm{g}}}{\rho_{\mathrm{l}}} dm_{\mathrm{l}} + \left(\left[1 - \frac{m_{\mathrm{l}}}{\rho_{\mathrm{l}}}\right](\rho_{\mathrm{g}})_p + \left[\frac{m_{\mathrm{l}}\rho_{\mathrm{g}}}{\rho_{\mathrm{l}}^2}\right](\rho_{\mathrm{l}})_p\right) dp. \end{aligned}$$

In other words, we have the relation

$$dp = \kappa(\rho_{\mathrm{l}} dm_{\mathrm{g}} + \rho_{\mathrm{g}} dm_{\mathrm{l}}), \tag{36}$$

where

$$\kappa = \frac{1}{\frac{\partial \rho_{\mathrm{l}}}{\partial p}\alpha_{\mathrm{l}}\rho_{\mathrm{g}} + \frac{\partial \rho_{\mathrm{g}}}{\partial p}\alpha_{\mathrm{g}}\rho_{\mathrm{l}}}.$$

Moreover, noting that the relation (13) can be written on the form

$$m_{\mathrm{g}} = m_{\mathrm{g}}(\alpha_{\mathrm{l}}, p) = (1 - \alpha_{\mathrm{l}})\rho_{\mathrm{g}}(p),$$

we see that

$$\begin{aligned} dm_{\mathrm{g}} &= (m_{\mathrm{g}})_{\alpha_{\mathrm{l}}} d\alpha_{\mathrm{l}} + (m_{\mathrm{g}})_p dp \\ &= -\rho_{\mathrm{g}} d\alpha_{\mathrm{l}} + (m_{\mathrm{g}})_p dp. \end{aligned}$$

Using (36), this relation can be rewritten as

$$\begin{aligned} d\alpha_{\mathrm{l}} &= \kappa\alpha_{\mathrm{g}}(\rho_{\mathrm{g}})_p dm_{\mathrm{l}} + \left(\alpha_{\mathrm{g}}\frac{\rho_{\mathrm{l}}}{\rho_{\mathrm{g}}}(\rho_{\mathrm{g}})_p\kappa - \frac{1}{\rho_{\mathrm{g}}}\right) dm_{\mathrm{g}} \\ &= \kappa\Big(\alpha_{\mathrm{g}}(\rho_{\mathrm{g}})_p dm_{\mathrm{l}} - \alpha_{\mathrm{l}}(\rho_{\mathrm{l}})_p dm_{\mathrm{g}}\Big). \end{aligned}$$

In other words, we have

$$d\alpha_{\mathrm{l}} = \kappa(-\frac{\partial \rho_{\mathrm{l}}}{\partial p}\alpha_{\mathrm{l}} dm_{\mathrm{g}} + \frac{\partial \rho_{\mathrm{g}}}{\partial p}\alpha_{\mathrm{g}} dm_{\mathrm{l}}). \tag{37}$$

By combining (36) and (37) we can write the masses in terms of a "pressure" and a "volume fraction" component as follows:

$$dm_{\mathrm{g}} = \alpha_{\mathrm{g}}\frac{\partial \rho_{\mathrm{g}}}{\partial p} dp - \rho_{\mathrm{g}} d\alpha_{\mathrm{l}} \tag{38}$$

and

$$dm_{\mathrm{l}} = \alpha_{\mathrm{l}}\frac{\partial \rho_{\mathrm{l}}}{\partial p} dp + \rho_{\mathrm{l}} d\alpha_{\mathrm{l}}. \tag{39}$$

The relations (36) and (37) reflect that differentials of the primitive variables α_{l} and p generally depend strongly on properties of the mixture of both masses through the differentials dm_{g} and dm_{l}. We recall from Section 3.1 that the AUSMD scheme is derived with the motivation of obtaining an accurate resolution of a discontinuity in the volume fraction variable, with the assumption of *equal* pressure. The derived mass fluxes do not take into consideration the effect of a *varying* pressure, and for the numerical experiments in Section 4 spurious oscillations were observed near discontinuities in the volume fraction variable. We want to take this aspect into account in the proposed modification of AUSMD. More specifically, we shall derive numerical mass fluxes which are consistent with the differential relations (36)–(39).

Related to this, we may also recall that the eigenstructure of the system is such that the pressure is commonly associated with fast-moving waves and the volume fraction is associated with slow-moving waves. This suggests that we should solve the pressure with a more robust scheme, where the numerical dissipation is increased to be in accordance with the faster velocity of the sonic

waves whereas for the slow volume fraction wave we should use a numerical flux whose numerical dissipation is low. In the next section we try to implement this understanding is a specific sense.

5.2. **Outline of the MF method.** With the above two observations in hand we will now describe an approach consisting of basically two main steps; the first step deals with the calculation of the cell interface pressure $p_{j+1/2}$ (Observation 1) whereas the second deals with the calculation of the cell center pressure p_j from the masses $m_{k,j}$ via (13). The essential part of the second step is to develop numerical mass fluxes which are consistent with Observation 2.

Note that step (I) deals with the pressure splittings whereas step (II) deals with the convective splittings.

(I) *Derivation of an evolution equation for the pressure $p_{j+1/2}$ at the cell interface.* The purpose of this pressure equation is to allow the pressure p and the momentum $\rho_k\alpha_k v_k$ to develop in a coherent manner. Particularly, we obtain a stronger coupling between the pressure and velocity fields than was the case for the pressure splittings used in the previous AUSM-type schemes [17, 9]. Increased robustness is the motivation behind our present approach.

By splitting the pressure based on an evolution equation, we honor time-tested traditions (see for instance [2]). However, by means of the *mixture fluxes* defined below, several new aspects are introduced.

(IIa) *Derivation of mixture mass fluxes appropriate for solving for $m_{k,j}$ from the mass equations.* This step involves the construction of *mixture mass fluxes* which are motivated by the relations (36) and (37). In particular, we introduce flux components F_k^D associated with sonic waves and F_k^A associated with volume fraction waves.

(IIb) *Specification of appropriate choices for F_k^D and F_k^A*

- F_k^D: The calculation of this mass flux component should be tightly coupled with the calculation of the cell interface pressure $p_{j+1/2}$ obtained from the pressure equation. This step ensures that $p_{j+1/2}$ and p_j will follow a concurrent time development, and this is important in order to avoid oscillations around the slow-moving volume fraction waves.
- F_k^A: The construction of this mass flux component should be chosen such that an accurate resolution of volume fraction waves is ensured.

We now describe a fully discrete implementation of the above algorithm. Given a uniform grid with time step Δt and spatial mesh grid size Δx, we can define an approximation $\mathbf{U}_j^{n+1}$ of $\mathbf{U}(x_j, t^{n+1})$ by the following three step algorithm:

Step I: The Pressure Evolution Equation. Discretizing the equation (34) by a staggered Lax-Friedrichs type of scheme we obtain

$$\frac{p_{j+1/2}^{n+1} - \frac{1}{2}(p_j^n + p_{j+1}^n)}{\Delta t} = -(\kappa\rho_{\mathrm{l}})_{j+1/2}^n \frac{I_{\mathrm{g},j+1}^n - I_{\mathrm{g},j}^n}{\Delta x} - (\kappa\rho_{\mathrm{g}})_{j+1/2}^n \frac{I_{\mathrm{l},j+1}^n - I_{\mathrm{l},j}^n}{\Delta x} \tag{40}$$

where we use the shorthand

$$I_k = m_k v_k .$$

This cell interface pressure $p_{j+1/2}^{n+1}$ is then used in the momentum equations of (31) as follows

$$\frac{I_{\mathrm{g},j}^{n+1} - I_{\mathrm{g},j}^n}{\Delta t} = -\delta_x \left(\rho_{\mathrm{g}}\alpha_{\mathrm{g}} v_{\mathrm{g}}^2\right)_j^n - (\Delta p)_j^n \, \delta_x(\alpha_{\mathrm{g}})_j^n - (\alpha_{\mathrm{g}})_j^n \frac{p_{j+1/2}^{n+1} - p_{j-1/2}^{n+1}}{\Delta x} + (Q_{\mathrm{g}})_j^n \tag{41}$$

$$\frac{I_{\mathrm{l},j}^{n+1} - I_{\mathrm{l},j}^n}{\Delta t} = -\delta_x \left(\rho_{\mathrm{l}}\alpha_{\mathrm{l}} v_{\mathrm{l}}^2\right)_j^n - (\Delta p)_j^n \, \delta_x(\alpha_{\mathrm{l}})_j^n - (\alpha_{\mathrm{l}})_j^n \frac{p_{j+1/2}^{n+1} - p_{j-1/2}^{n+1}}{\Delta x} + (Q_{\mathrm{l}})_j^n . \tag{42}$$

Here δ_x represents the operator

$$\delta_x w_j = \frac{w_{j+1/2} - w_{j-1/2}}{\Delta x}. \tag{43}$$

For the numerical fluxes $(\rho_k \alpha_k v_k^2)_{j+1/2}$ we employ the AUSMD fluxes as described by (15)–(19). For the numerical flux $(\alpha_k)_{j+1/2}$ we use a central discretization as follows

$$(\alpha_k)_{j+1/2} = \frac{1}{2}\left(\alpha_{k,j} + \alpha_{k,j+1}\right). \tag{44}$$

In this respect we follow in the footsteps of Coquel et al [3] and Paillère et al [17]. In particular, this simple treatment is independent of the splitting formulas $P^{\pm}$ given by (23).

Note that the cell interface pressure $p_{j+1/2}^{n+1}$ can be written on the viscous form

$$\begin{aligned} p_{j+1/2}^{n+1} &= P(\mathbf{U}_j^n, \mathbf{U}_{j+1}^n) \\ &= \frac{1}{2}\left(p_j^n + p_{j+1}^n\right) - \left[D_{\mathrm{g},j+1/2}^n (I_{g,j+1}^n - I_{g,j}^n) + D_{\mathrm{l},j+1/2}^n (I_{l,j+1}^n - I_{l,j}^n)\right] \end{aligned} \tag{45}$$

where the numerical viscosity coefficients $D_{k,j+1/2}^n$ are given by

$$D_{\mathrm{g},j+1/2}^n = \frac{\Delta t}{\Delta x} \kappa_{j+1/2}^n \rho_{\mathrm{l},j+1/2}^n. \tag{46}$$

and

$$D_{\mathrm{l},j+1/2}^n = \frac{\Delta t}{\Delta x} \kappa_{j+1/2}^n \rho_{\mathrm{g},j+1/2}^n. \tag{47}$$

Interface values $(\cdot)_{j+1/2}^n$ needed for the coefficients (46) and (47) are obtained by using $p_{j+1/2}^n$ (which has been calculated from (40) at the previous timestep) and $\alpha_{j+1/2}^n$ defined as the arithmetic average

$$\alpha_{j+1/2}^n = \frac{1}{2}(\alpha_j^n + \alpha_{j+1}^n).$$

Remark 5. *We note that the role of the non-conservative pressure evolution equation* (40) *is simply to define an appropriate numerical flux* $p_{j+1/2} = P(\mathbf{U}_j, \mathbf{U}_{j+1})$ *for the discretization of the pressure term in* (41) *and* (42). *From* (45) *we easily see that this numerical flux is consistent with the physical flux, i.e.* $P(\mathbf{U}, \mathbf{U}) = p$ *for all* $\mathbf{U}$.

Remark 6. *Other choices for the discretization of the pressure evolution equation* (34) *than the one given by* (40) *would of course be possible. One natural choice could be to consider*

$$\frac{p_{j+1/2}^{n+1} - p_{j+1/2}^n}{\Delta t} = -(\kappa\rho_l)_{j+1/2}^n \frac{I_{\mathrm{g},j+1}^n - I_{\mathrm{g},j}^n}{\Delta x} - (\kappa\rho_g)_{j+1/2}^n \frac{I_{\mathrm{l},j+1}^n - I_{\mathrm{l},j}^n}{\Delta x}. \tag{48}$$

We will refer to this as the FTCS (forward time, centered space) scheme. Now the consistency relation (45) *between the interface pressure* $p_{j+1/2}$ *and cell center pressure* p_j *no longer holds, and there is no obvious mechanism that drives the difference between these two pressures to zero. Note also that there is no numerical dissipation terms associated with the discretization of* $\partial_x I_k$ *in* (48), *whereas such dissipation terms may be introduced in* (45) *through the term* $(p_j^n + p_{j+1}^n)/2$. *In the numerical section we explore these two different discretizations of the pressure evolution equation in order to shed light on the importance of a consistent treatment of* p_j *and* $p_{j+1/2}$.

Step IIa: Construction of Mixture Mass Fluxes. What remains to be solved for now is the masses $m_{k,j}^{n+1}$ through a proper discretization of the mass conservation equations of (31). We consider a general discretization

$$\frac{m_{k,j}^{n+1} - m_{k,j}^n}{\Delta t} = -\frac{1}{\Delta x}\Big(F_{k,j+1/2}^n - F_{k,j-1/2}^n\Big), \tag{49}$$

where $F_{k,j+1/2} = F_k(U_j, U_{j+1})$ is the numerical mass flux at cell interface $j+1/2$ corresponding to the physical flux $f_k(U) = \rho_k \alpha_k v_k$. From (38) and (39) we see that the mass differentials dm_k can be splitted in a pressure component dp and a volume fraction component $d\alpha$. We now want to design a numerical flux which is consistent with this splitting, i.e. we introduce a flux component F_p and F_α such that the mass fluxes F_{l} and F_{g} are given by

$$F_{\mathrm{l}} = \alpha_{\mathrm{l}} \frac{\partial \rho_{\mathrm{l}}}{\partial p} F_p + \rho_{\mathrm{l}} F_\alpha \tag{50}$$

and

$$F_{\rm g} = \alpha_{\rm g}\frac{\partial \rho_{\rm g}}{\partial p}F_p - \rho_{\rm g}F_\alpha. \tag{51}$$

The flux component F_p is associated with the pressure, hence we want to assign a diffusive mass flux $F^{\rm D}$ for stable approximation of pressure for all waves. Inspired by the differential relation (36) we propose to give F_p the following form

$$F_p = \kappa\rho_{\rm g}F_{\rm l}^{\rm D} + \kappa\rho_{\rm l}F_{\rm g}^{\rm D} \tag{52}$$

Similarly, the flux component F_α is associated with the volume fraction, hence we want to assign an accurate mass flux $F^{\rm A}$. Inspired by the differential relation (37), we propose to give F_α the following form

$$F_\alpha = \kappa\frac{\partial \rho_{\rm g}}{\partial p}\alpha_{\rm g}F_{\rm l}^{\rm A} - \kappa\frac{\partial \rho_{\rm l}}{\partial p}\alpha_{\rm l}F_{\rm g}^{\rm A}. \tag{53}$$

Here we note that a subscript $j+1/2$ is assumed on the fluxes and coefficients. Substituting (52) and (53) into (51) and (50) we obtain the final hybrid mass fluxes

$$F_{\rm l} = \kappa\left(\rho_{\rm g}\alpha_{\rm l}\frac{\partial \rho_{\rm l}}{\partial p}F_{\rm l}^{\rm D} + \rho_{\rm l}\alpha_{\rm g}\frac{\partial \rho_{\rm g}}{\partial p}F_{\rm l}^{\rm A} + \rho_{\rm l}\alpha_{\rm l}\frac{\partial \rho_{\rm l}}{\partial p}(F_{\rm g}^{\rm D} - F_{\rm g}^{\rm A})\right) \tag{54}$$

and

$$F_{\rm g} = \kappa\left(\rho_{\rm l}\alpha_{\rm g}\frac{\partial \rho_{\rm g}}{\partial p}F_{\rm g}^{\rm D} + \rho_{\rm g}\alpha_{\rm l}\frac{\partial \rho_{\rm l}}{\partial p}F_{\rm g}^{\rm A} + \rho_{\rm g}\alpha_{\rm g}\frac{\partial \rho_{\rm g}}{\partial p}(F_{\rm l}^{\rm D} - F_{\rm l}^{\rm A})\right) \tag{55}$$

The coefficient variables at $j+1/2$ remain to be determined. Consistent with the treatment of the coefficients of the pressure evolution equation (45) we suggest finding these from the cell interface pressure $p_{j+1/2}$ as well as the relation

$$\alpha_{j+1/2} = \frac{1}{2}(\alpha_j + \alpha_{j+1}).$$

Remark 7. *We remark that the consistency criterion*

$$F_k(U,U) = f_k(U) = \rho_k\alpha_k v_k, \tag{56}$$

relating the numerical flux F_k to the physical flux f_k, is satisfied for the hybrid fluxes (54) and (55) provided the fluxes F_k^A and F_k^D are consistent. In particular if $F_k^A = F_k^D$ the expressions (54) and (55) reduce to the trivial identity

$$F_k = F_k^A = F_k^D. \tag{57}$$

Step IIb: Specification of Mass Flux Components F_k^D and F_k^A.

F_k^D-component. The purpose of this flux component is to ensure consistency between calculation of masses and the pressure calculation and by that ensure stable (non-oscillatory) approximations of slow moving volume fraction waves. Going back to the pressure equation (40), we see that it naturally defines a conservative scheme for calculating masses at $j+1/2$ as

$$\frac{m_{k,j+1/2}^{n+1} - \frac{1}{2}\left(m_{k,j}^n + m_{k,j+1}^n\right)}{\Delta t} + \frac{I_{k,j+1}^n - I_{k,j}^n}{\Delta x} = 0. \tag{58}$$

If we now compute the simple average

$$m_{k,j} = \frac{1}{2}\left(m_{k,j-1/2} + m_{k,j+1/2}\right) \tag{59}$$

and substitute (58), we obtain the following difference equation for $m_{k,j}$

$$\frac{m_{k,j}^{n+1} - \frac{1}{4}\left(2m_{k,j}^n + m_{k,j-1}^n + m_{k,j+1}^n\right)}{\Delta t} + \frac{1}{2\Delta x}\left(I_{k,j+1}^n - I_{k,j-1}^n\right) = 0, \tag{60}$$

which can be written on flux-conservative form (49) with the numerical fluxes

$$F_{k,j+1/2}^{\rm D} = F_k^{\rm D}(\mathbf{U}_j, \mathbf{U}_{j+1}) = \frac{1}{2}(I_{k,j} + I_{k,j+1}) + \frac{1}{4}\frac{\Delta x}{\Delta t}(m_{k,j} - m_{k,j+1}). \tag{61}$$

Now we may solve for the masses $m_{k,j}$ using the fluxes (61), taking advantage of the stabilizing effect given by their interdependence of the cell interface pressure $p_{j+1/2}$ through $I_{k,j}$ and $I_{k,j+1}$.

F_k^A-component. The purpose of this flux component is to ensure accurate resolution of slow-moving volume fraction waves (mass fronts). As demonstrated in Section 4 the AUSMD mass fluxes give a resolution of such waves comparable to that of the Roe scheme. Hence, we propose to identify F_k^A with the AUSMD mass fluxes given in Section 3.1 and defined by (15) and (17)–(19). We expect that other choices also would be possible, e.g. the AUSM$^+$ flux of Paillère et al [17]. This will be explored elsewhere.

Remark 8. *The fluxes (61) are central and hence highly diffusive. Consequently the fluxes (61) will produce highly inaccurate solutions to slow volume fraction fronts. Therefore we wish to hybridize the flux (61) with a more accurate flux F^A via the mixture fluxes* (54) *and* (55) *such that we maintain the stability of (61) for the pressure variable while falling back to the accuracy of F^A on the volume fraction waves.*

5.3. **MF-AUSMD.** We now summarize the numerical scheme just derived, referred to as the *MF-AUSMD* (Mixture Fluxes based on AUSMD) scheme. Let δ_x be defined as in (43).

Mass Equations. We discretize the mass equations as follows

$$\frac{m_{k,j}^{n+1} - m_{k,j}^n}{\Delta t} = -\delta_x F_{k,j}^n,$$

where the mass fluxes $F_{k,j+1/2}$ are given by

$$F_{\rm l} = \kappa \left(\rho_{\rm g}\alpha_{\rm l} \frac{\partial \rho_{\rm l}}{\partial p} F_{\rm l}^{\rm D} + \rho_{\rm l}\alpha_{\rm g} \frac{\partial \rho_{\rm g}}{\partial p} F_{\rm l}^{\rm A} + \rho_{\rm l}\alpha_{\rm l} \frac{\partial \rho_{\rm l}}{\partial p} (F_{\rm g}^{\rm D} - F_{\rm g}^{\rm A}) \right)$$

and

$$F_{\rm g} = \kappa \left(\rho_{\rm l}\alpha_{\rm g} \frac{\partial \rho_{\rm g}}{\partial p} F_{\rm g}^{\rm D} + \rho_{\rm g}\alpha_{\rm l} \frac{\partial \rho_{\rm l}}{\partial p} F_{\rm g}^{\rm A} + \rho_{\rm g}\alpha_{\rm g} \frac{\partial \rho_{\rm g}}{\partial p} (F_{\rm l}^{\rm D} - F_{\rm l}^{\rm A}) \right)$$

as described in Step IIa. Here

$$F_{k,j+1/2}^{\rm D} = \frac{1}{2}(I_{k,j} + I_{k,j+1}) + \frac{1}{4}\frac{\Delta x}{\Delta t}(m_{k,j} - m_{k,j+1}), \qquad m_k = \rho_k \alpha_k, \qquad I_k = m_k v_k$$

and

$$F_{k,j+1/2}^{\rm A} = (\rho_k \alpha_k v_k)_{j+1/2}^{\rm AUSMD}$$

as described in Section 3.1.

Momentum Equations. We discretize the momentum equations as follows

$$\frac{I_{k,j}^{n+1} - I_{k,j}^n}{\Delta t} = -\delta_x \left(\rho_k \alpha_k v_k^2\right)_j^n - (\Delta p)_j^n \, \delta_x(\alpha_k)_j^n - (\alpha_k)_j^n \delta_x \, (p)_j^* + (Q_{\rm g})_j^n.$$

Here

$$(\alpha_k)_{j+1/2} = \frac{1}{2}\left(\alpha_{k,j} + \alpha_{k,j+1}\right)$$

and

$$p_{j+1/2}^* = \frac{1}{2}\left(p_j + p_{j+1}\right) - \Delta t (\kappa\rho_{\rm l})_{j+1/2} \frac{I_{{\rm g},j+1} - I_{{\rm g},j}}{\Delta x} - \Delta t (\kappa\rho_{\rm g})_{j+1/2} \frac{I_{{\rm l},j+1} - I_{{\rm l},j}}{\Delta x}$$

as described in Step I. Finally

$$\left(\rho_k \alpha_k v_k^2\right)_{j+1/2} = \left(\rho_k \alpha_k v_k^2\right)_{j+1/2}^{\rm AUSMD}$$

as described in Section 3.1.

6. Basic properties possessed by the Mixture Flux AUSMD scheme

In this section we want to verify that the proposed MF-AUSMD scheme possesses certain basic accuracy and stability properties known from the literature.

6.1. **Accurate approximation of steady and moving contact discontinuities.** We will now investigate how this Mixture Flux method is related to the AUSM (Advection Upstream Splitting Method) framework of Liou et al [12, 13, 30] regarding the performance on a moving or stationary contact discontinuity. For this purpose we consider the contact discontinuity given by

$$\begin{aligned} p_{\mathrm{L}} &= p_{\mathrm{R}} = p \\ \alpha_{\mathrm{L}} &\neq \alpha_{\mathrm{R}} \\ (v_{\mathrm{g}})_{\mathrm{L}} = (v_{\mathrm{l}})_{\mathrm{L}} &= (v_{\mathrm{g}})_{\mathrm{R}} = (v_{\mathrm{l}})_{\mathrm{R}} = v. \end{aligned} \tag{62}$$

All pressure terms vanish from the model (4)-(7), and it is seen that the solution to this initial value problem is simply that the discontinuity will propagate with the velocity v. The exact solution of the Riemann problem will then give the numerical mass flux

$$(\rho\alpha v)_{j+1/2} = \frac{1}{2}\rho(\alpha_{\mathrm{L}} + \alpha_{\mathrm{R}})v - \frac{1}{2}\rho(\alpha_{\mathrm{R}} - \alpha_{\mathrm{L}})|v|. \tag{63}$$

As remarked in Section 3.1 AUSMD mass fluxes take this form for the contact discontinuity (62). Now we want to find a criterion for the F_k^D flux components that ensures that the mixture mass fluxes (54) and (55) also will possess this good feature.

In particular, we note that the pressure will remain constant and uniform as the discontinuity is propagating. Consequently a natural requirement on a "good" flux F_k^{D} for stable pressure resolution is that it preserves the constancy of pressure for the moving or stationary contact discontinuity given by (62).

We write (36) as

$$dp = \kappa d\mu \tag{64}$$

where

$$d\mu = \rho_{\mathrm{g}} dm_{\mathrm{l}} + \rho_{\mathrm{l}} dm_{\mathrm{g}}. \tag{65}$$

To maintain a constant pressure we must have $d\mu = 0$. Assuming constant pressure, (65) can be integrated to yield

$$\mu = \rho_{\mathrm{g}} m_{\mathrm{l}} + \rho_{\mathrm{l}} m_{\mathrm{g}} = \rho_{\mathrm{g}}\rho_{\mathrm{l}}(\alpha_{\mathrm{l}} + \alpha_{\mathrm{g}}) = \rho_{\mathrm{g}}\rho_{\mathrm{l}}.$$

To maintain constancy of μ and hence p we now insist that the flux F^{D} is a consistent numerical flux when applied to the mix mass μ. That is, we impose

$$\rho_{\mathrm{g}} F_{\mathrm{l}}^{\mathrm{D}} + \rho_{\mathrm{l}} F_{\mathrm{g}}^{\mathrm{D}} = \rho_{\mathrm{g}}\rho_{\mathrm{l}} v. \tag{66}$$

for the contact discontinuity (62).

Definition 1. *A pair of numerical fluxes F_{l} and F_{g} that satisfy (66) for the contact discontinuity (62) will in the following be termed "pressure coherent" fluxes.*

We note that the van Leer mass fluxes given by (15) and (14) as well as the upwind fluxes (63) are pressure coherent. However, we can easily construct a pair of perfectly valid mass fluxes that are *not* pressure coherent. Consider for example the stationary contact discontinuity (62) with $v = 0$. Let F_{g} be given by the upwind flux (63) and F_{l} be given by the van Leer flux (15). Then

$$\rho_{\mathrm{g}} F_{\mathrm{l}} + \rho_{\mathrm{l}} F_{\mathrm{g}} = \rho_{\mathrm{g}}\rho_{\mathrm{l}} \frac{c}{4} \left((\alpha_{\mathrm{l}})_{\mathrm{L}} - (\alpha_{\mathrm{l}})_{\mathrm{R}}\right) \neq 0,$$

not satisfying the requirement (66).

We now state the following lemma relevant for schemes obtained by using the Mixture Flux method.

Lemma 1. *Let the mixture fluxes (54) and (55) be constructed from pressure coherent fluxes F_k^D, and fluxes F_k^A that reduce to the upwind fluxes (63) on a contact discontinuity of the form (62). Then the hybrid fluxes (54) and (55) also reduce to the upwind fluxes (63) on the contact discontinuity (62).*

Proof. We consider the hybrid liquid mass flux (54) and assume that $v \geq 0$. Remembering that a subscript $j+1/2$ is assumed on the variables, we write the flux as

$$F_{\mathrm{l}} = \kappa \left(\alpha_{\mathrm{l}} \frac{\partial \rho_{\mathrm{l}}}{\partial p} (\rho_{\mathrm{g}} F_{\mathrm{l}}^{\mathrm{D}} + \rho_{\mathrm{l}} F_{\mathrm{g}}^{\mathrm{D}}) + \rho_{\mathrm{l}} \alpha_{\mathrm{g}} \frac{\partial \rho_{\mathrm{g}}}{\partial p} F_{\mathrm{l}}^{\mathrm{A}} - \rho_{\mathrm{l}} \alpha_{\mathrm{l}} \frac{\partial \rho_{\mathrm{l}}}{\partial p} F_{\mathrm{g}}^{\mathrm{A}} \right). \tag{67}$$

Using the required properties of F_k^{D} and F_k^{A} we obtain

$$F_{\mathrm{l}} = \kappa \left(\alpha_{\mathrm{l}} \frac{\partial \rho_{\mathrm{l}}}{\partial p} \rho_{\mathrm{g}} \rho_{\mathrm{l}} v + \rho_{\mathrm{l}}^2 \alpha_{\mathrm{g}} \frac{\partial \rho_{\mathrm{g}}}{\partial p} (\alpha_{\mathrm{l}})_{\mathrm{L}} v - \rho_{\mathrm{g}} \rho_{\mathrm{l}} \alpha_{\mathrm{l}} \frac{\partial \rho_{\mathrm{l}}}{\partial p} (1 - (\alpha_{\mathrm{l}})_{\mathrm{L}}) v \right) = \rho_{\mathrm{l}} (\alpha_{\mathrm{l}})_{\mathrm{L}} v, \tag{68}$$

where we have used that

$$\rho_{j+1/2} = \rho_j = \rho_{j+1} \tag{69}$$

which follows from the assumption of constant, uniform pressure. Spatial and phasic symmetry directly give the corresponding results for F_{g} and $v \leq 0$, completing the proof. □

In view of Lemma 1 we obtain the following result for the MF-AUSMD scheme.

Proposition 1. *The mass fluxes of the MF-AUSMD scheme described in Section 5.3 reduce to the upwind fluxes (63) on a contact discontinuity of the form (62).*

Proof. In view of Section 3.1.2 we know that the F_k^{A} components in the MF-AUSMD scheme reduce to the upwind fluxes (63) on a contact discontinuity of the form (62). Thus, we only need to check that the F_k^{D} components given by (61) are pressure coherent in the sense of Definition 1 and then appeal to Lemma 1. Substituting constant pressure and velocities in (61) we get

$$\begin{aligned} \rho_{\mathrm{g}} F_{\mathrm{l}}^D + \rho_{\mathrm{l}} F_{\mathrm{g}}^D &= \rho_{\mathrm{g}} \rho_{\mathrm{l}} \left[\frac{v}{2} (\alpha_{\mathrm{l},j} + \alpha_{\mathrm{l},j+1}) + \frac{\Delta x}{4\Delta t} (\alpha_{\mathrm{l},j} - \alpha_{\mathrm{l},j+1}) \right] \\ &\quad + \rho_{\mathrm{g}} \rho_{\mathrm{l}} \left[\frac{v}{2} (\alpha_{\mathrm{g},j} + \alpha_{\mathrm{g},j+1}) + \frac{\Delta x}{4\Delta t} (\alpha_{\mathrm{g},j} - \alpha_{\mathrm{g},j+1}) \right] \\ &= \rho_{\mathrm{g}} \rho_{\mathrm{l}} \left[\frac{v}{2} (1+1) + \frac{\Delta x}{4\Delta t} (1-1) \right] = \rho_{\mathrm{g}} \rho_{\mathrm{l}} v. \end{aligned}$$

□

This result illustrates that the Mixture Flux method presented here is a close relative to the AUSMV/D philosophy of Wada and Liou [30], as it achieves the same goal of accurately resolving moving or stationary contact discontinuities. A notable difference is that the AUSMV/D framework combines velocity splitting formulas, whereas the MF method presented here combines numerical fluxes directly and thereby enforces a much stronger coupling between the various equations.

6.2. **Abgrall's principle.** According to the principle due to Abgrall [1, 22, 23] it is desirable that the numerical scheme respects the following physical principle:
A flow, uniform in pressure and velocity must remain uniform in the same variables during its time evolution.
In other words, if we had constant pressure and velocity everywhere in a flow at the time level t^n, then we will get the same pressure and velocity at the time t^{n+1}.

We now check if the MF-AUSMD scheme obeys Abgrall's priciple. Consequently, we assume that we have the contact discontinuity given by (62) and that it remains unchanged during the time interval $[t^n, t^{n+1}]$. In view of Proposition 1 and the fact that the convective fluxes of the momentum equations are based on (16), we immediately conclude that the mass equations (49) and the momentum equations (41) and (42) take the form

$$\begin{aligned} (\rho\alpha)_j^{n+1} &= (\rho\alpha)_j^n - \frac{\Delta t}{\Delta x} \left((\rho\alpha v)_{j+1/2}^n - (\rho\alpha v)_{j-1/2}^n \right) \\ v(\rho\alpha)_j^{n+1} &= v(\rho\alpha)_j^n - v\frac{\Delta t}{\Delta x} \left((\rho\alpha v)_{j+1/2}^n - (\rho\alpha v)_{j-1/2}^n \right) \\ &\quad - (\Delta p)_j^n \frac{\Delta t}{2\Delta x} (\alpha_{j+1}^n - \alpha_{j-1}^n) - \alpha_j^n \frac{\Delta t}{\Delta x} (p_{j+1/2}^{n+1} - p_{j-1/2}^{n+1}), \end{aligned}$$

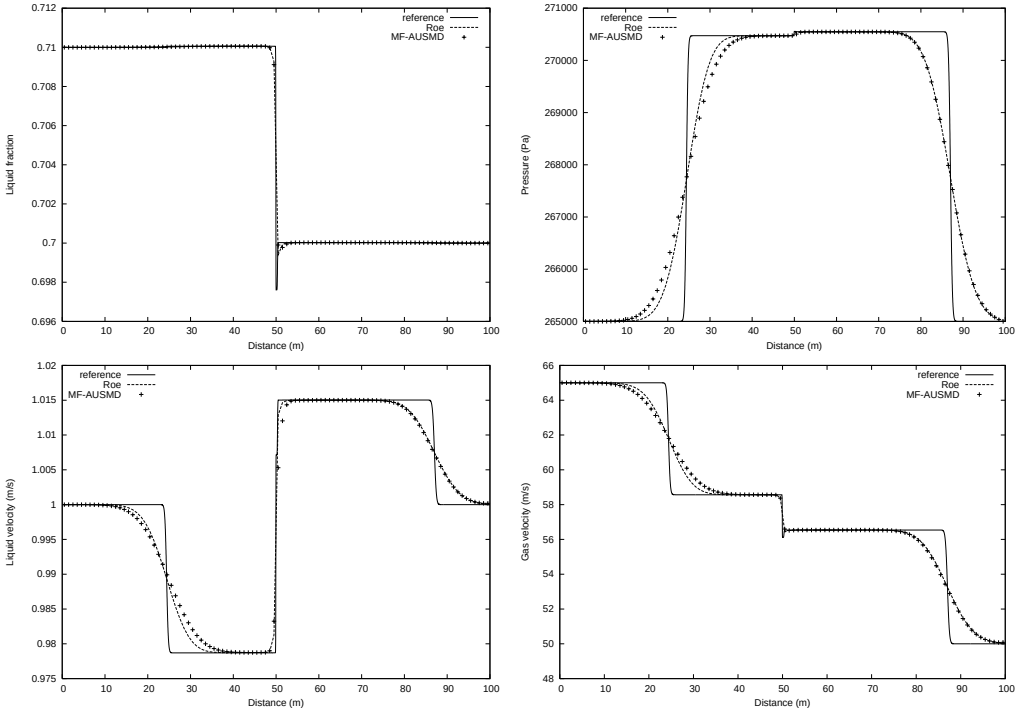

FIGURE 3. LRV shock tube problem, $T = 0.1$ s, 100 grid cells. MF-AUSMD vs Roe scheme. Top left: Liquid fraction. Top right: Pressure. Bottom left: Liquid velocity: Bottom right: Gas velocity.

where $(\rho\alpha v)^n_{j+1/2}$ is on the form (63). From (11) we conclude that $(\Delta p)^n_j = 0$. Referring to (45) we also see that $p^{n+1}_{j+1/2}$ reduces to

$$p^{n+1}_{j+1/2} = p - \kappa^n_{j+1/2}\frac{\Delta t}{\Delta x}\left[\rho_{\rm l}\rho_{\rm g}v(\alpha_{{\rm g},j+1} - \alpha_{{\rm g},j}) + \rho_{\rm l}\rho_{\rm g}v(\alpha_{{\rm l},j+1} - \alpha_{{\rm l},j})\right] = p.$$

Consequently, the pressure terms vanish and we can conclude that the discretization of the MF-AUSMD satisfies Abgrall's principle.

7. Numerical Simulations

In the first example we seek to obtain some more detailed insight into the mechanisms of the MF method. Particularly, we focus on the two following points which constitute the heart of the MF approach: (i) The effect of using the mixture mass fluxes (54) and (55) obtained by mixing the F^D_k and the F^A_k components; (ii) The discretization of the pressure evolution equation (40).

The purpose of the rest of the section is to demonstrate the overall good approximation properties of the MF-AUSMD scheme by considering the performance for a series of various flow cases. In particular, we compare with the AUSMD and the Roe scheme used in Section 4. The purpose is to demonstrate that the MF-AUSMD scheme possesses stability properties similar to the Roe scheme and at the same time keeps the accuracy of the AUSMD scheme.

7.1. **Large Relative Velocity Shock.** We now revisit the LRV shock studied in Section 4.1.

7.1.1. *Test of stability and accuracy for MF-AUSMD.* We now aim to compare the MF-AUSMD scheme with the Roe scheme under equal conditions. As in Section 4.1, we assume a grid of 100 cells and a timestep of

$$\frac{\Delta x}{\Delta t} = 10^3 \text{ m/s}. \tag{70}$$

The results, plotted at the time $T = 0.1$ s, are given in Figure 3. As the figure indicates, the schemes

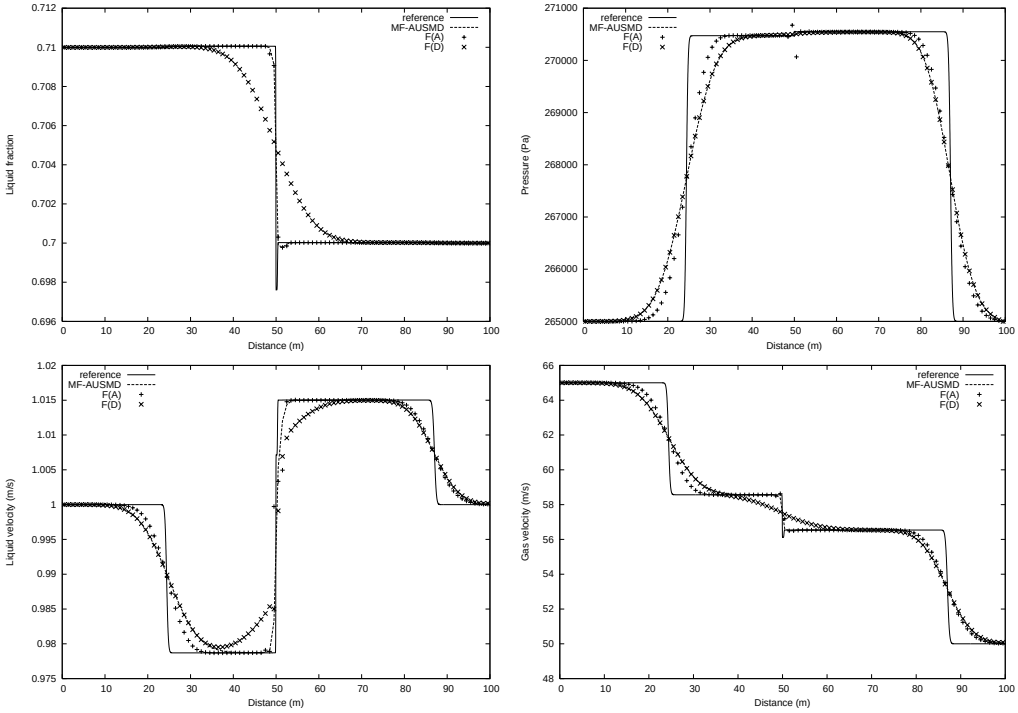

FIGURE 4. LRV shock tube problem, $T = 0.1$ s, 100 grid cells. MF-AUSMD vs the purely diffusive (F_k^{D}) and accurate (F_k^{A}) components. Top left: Liquid fraction. Top right: Pressure. Bottom left: Liquid velocity: Bottom right: Gas velocity.

are virtually inseparable on the resolution of the right-going sonic wave. On the left-going sonic wave, the MF-AUSMD scheme is slightly more diffusive than the Roe scheme. A comparison with the plot in Section 4.1 reveals that the MF-AUSMD scheme introduces somewhat more diffusion on this wave also compared to the AUSMD scheme. On the other hand, we note that the oscillatory behaviour of the original AUSMD scheme is completely absent, demonstrating the fruitfulness of the MF approach.

7.1.2. *Mixture mass fluxes versus single mass fluxes.* We now wish to illustrate more precisely the effect of introducing the mixture mass flux obtained by combining the two different flux components F_k^{D} and F_k^{A} as described by (54) and (55). For that purpose, we consider the following 3 schemes:

(1) The MF-AUSMD scheme.
(2) The scheme obtained by replacing the MF-AUSMD mass fluxes with the pure AUSMD fluxes F_k^{A}. This is denoted as the $F(A)$-scheme in Figure 4. Note that this is not identical to the AUSMD scheme of Section 3.1.2, as the discretization of the pressure term is different.
(3) The scheme obtained by replacing the MF-AUSMD mass fluxes with the pure diffusive mass fluxes F_k^{D} given by (61). This is denoted as the $F(D)$-scheme in Figure 4.

Results for 100 cells are given in Figure 4. We note the following:

- The $F(D)$-scheme is very stable but highly diffusive for the volume fraction wave, more diffusive than the van Leer scheme (compare with Figure 1 of Section 4.1).
- The $F(A)$-scheme is accurate on all waves, similar to the AUSMD scheme. However, the heavy oscillations observed for the liquid velocity for the AUSMD scheme (Figure 1 of Section 4.1), have been eliminated. This clearly is an effect of the use of the pressure

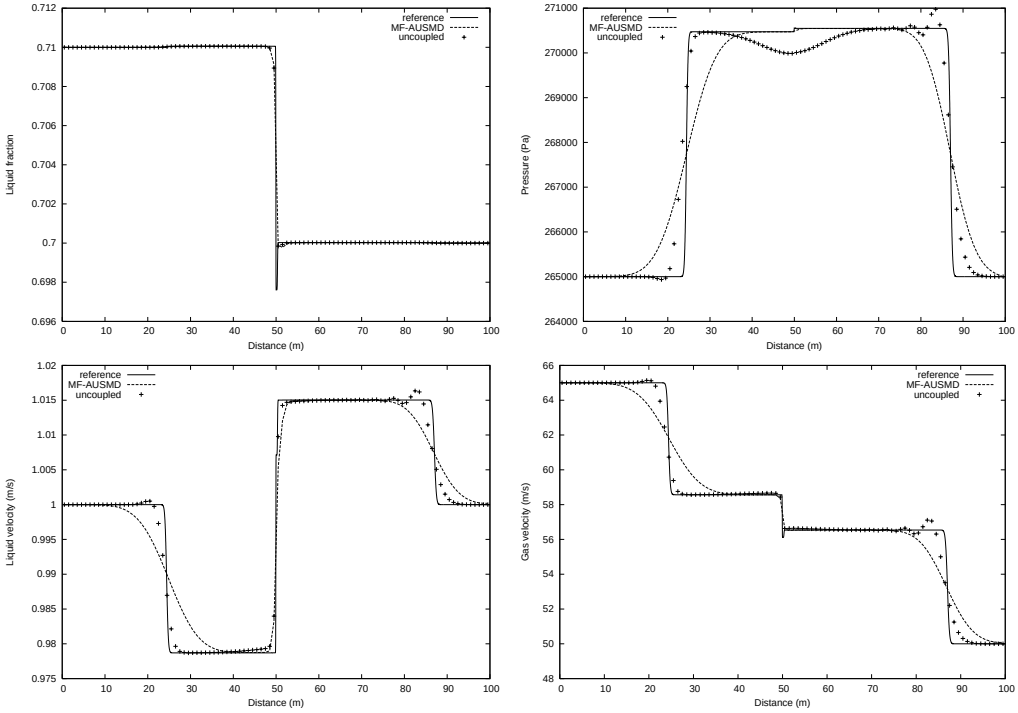

FIGURE 5. LRV shock tube problem, $T = 0.1$ s, 100 grid cells. Lax-Friedrichs based MF-AUSMD vs FTCS based MF-AUSMD. Top left: Liquid fraction. Top right: Pressure. Bottom left: Liquid velocity: Bottom right: Gas velocity.

evolution equation (40) in the discretization of the pressure terms of the momentum equations. However, the $F(A)$-scheme is not perfect as the oscillation for the pressure variable remains.

- The use of the mixture mass fluxes (54) and (55) in the MF-AUSMD scheme efficiently removes the oscillation observed for the pressure variable of the $F(A)$-scheme. The MF-AUSMD scheme really seems to combine the fluxes F_k^{A} and F_k^{D} in the desired way, giving results similar to F_k^{D} for fast waves and F_k^{A} for slow waves.
- The fact that MF-AUSMD is slightly more diffusive than AUSMD on the sonic waves seems to follow directly from the fact that F_k^{D} is slightly more diffusive than F_k^{A} on these waves.

7.1.3. *Comparison of two different discretizations of the pressure evolution equation* (34). We now compare the Lax-Friedrichs discretization of the cell interface pressure used in MF-AUSMD, with a modified variation where we use the FTCS scheme of Remark 6. This latter scheme implies that the cell interface pressure $p_{j+1/2}$ is uncoupled from the cell center pressure p_j. We keep the mass fluxes unchanged, using the mixture mass fluxes (54) and (55). Results are given in Figure 5. We note the following:

- The lack of a consistency mechanism between the cell interface pressure $p_{j+1/2}$ and the cell center pressure p_j produces a large undershoot in the pressure near $x = 50$ m where the volume fraction wave is located.
- The uncoupled scheme based on a FTCS pressure discretization produces a sharp resolution of the pressure waves. On the other hand, numerical oscillations are produced near the pressure discontinuities. As noted in Remark 6 the FTCS scheme has zero numerical viscosity, and will be unstable on a scalar equation (see for instance [25]). The result above indicates that a certain amount of numerical dissipation in the pressure equation is needed to stabilize the solution for sonic waves.

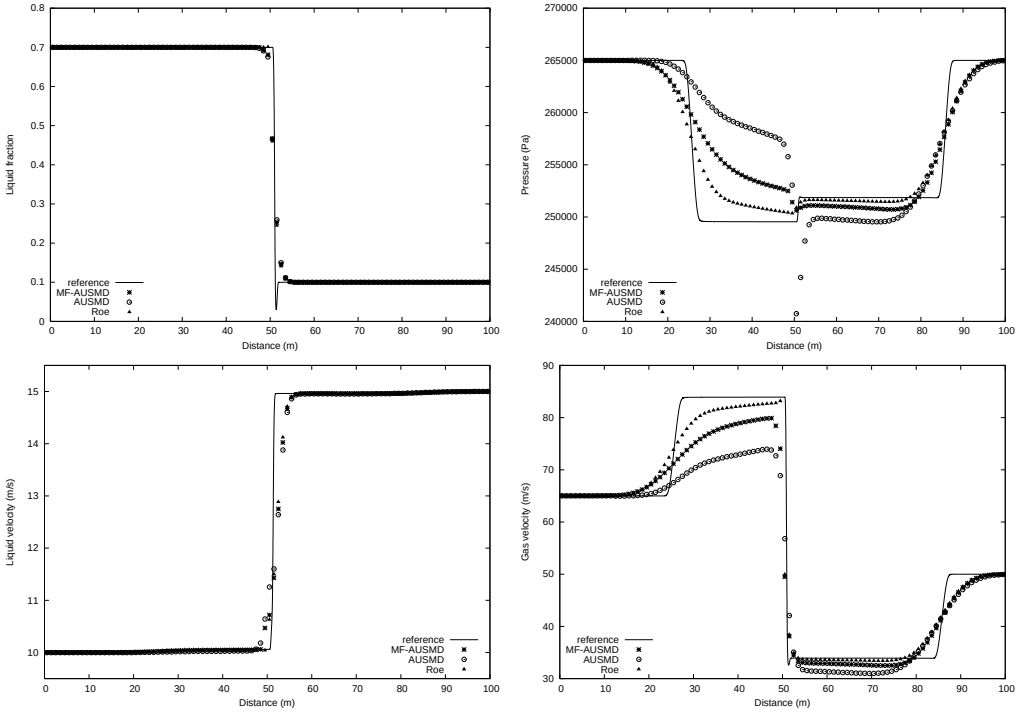

FIGURE 6. Modified LRV shock tube problem, $T = 0.1$ s, 100 grid cells. MF-AUSMD, AUSMD and Roe scheme. Top left: Gas fraction. Top right: Pressure. Bottom left: Liquid velocity: Bottom right: Gas velocity.

Remark 9. *Clearly, the discretization of the pressure evolution equation at the cell interface has a strong effect on the cell center pressures produced by the MF scheme. For the purposes of this paper, we prefer to stick to the Lax-Friedrichs discretization* (40)*, because of the simplicity and robustness of this scheme. In particular it allows for writing the cell interface pressure on a consistent, viscous form* (45) *in a straightforward manner. The numerical results indicate that other ways of discretizing the pressure equation could be explored with the possibility of improving the accuracy of the fast (sonic) waves.*

7.2. **Modified Large Relative Velocity Shock.** We consider a modified version of the LRV shock, where we introduce a jump in the liquid velocity as well as a larger jump in volume fraction. This problem was studied as shock tube problem 2 in [9].

The initial states are given by

$$\mathbf{W}_{\mathrm{L}} = \begin{bmatrix} p \\ \alpha_{\mathrm{l}} \\ v_{\mathrm{g}} \\ v_{\mathrm{l}} \end{bmatrix} = \begin{bmatrix} 265000\ \mathrm{Pa} \\ 0.7 \\ 65\ \mathrm{m/s} \\ 10\ \mathrm{m/s} \end{bmatrix} \tag{71}$$

and

$$\mathbf{W}_{\mathrm{R}} = \begin{bmatrix} p \\ \alpha_{\mathrm{l}} \\ v_{\mathrm{g}} \\ v_{\mathrm{l}} \end{bmatrix} = \begin{bmatrix} 265000\ \mathrm{Pa} \\ 0.1 \\ 50\ \mathrm{m/s} \\ 15\ \mathrm{m/s} \end{bmatrix}. \tag{72}$$

7.2.1. *Comparison between AUSMD, MF-AUSMD and Roe scheme.* Results after $T = 0.1$ s are given in Figure 6, using a grid of 100 cells and a timestep $\Delta x/\Delta t = 750$ m/s. The reference solution was calculated by the Roe scheme on a grid of 10 000 cells.

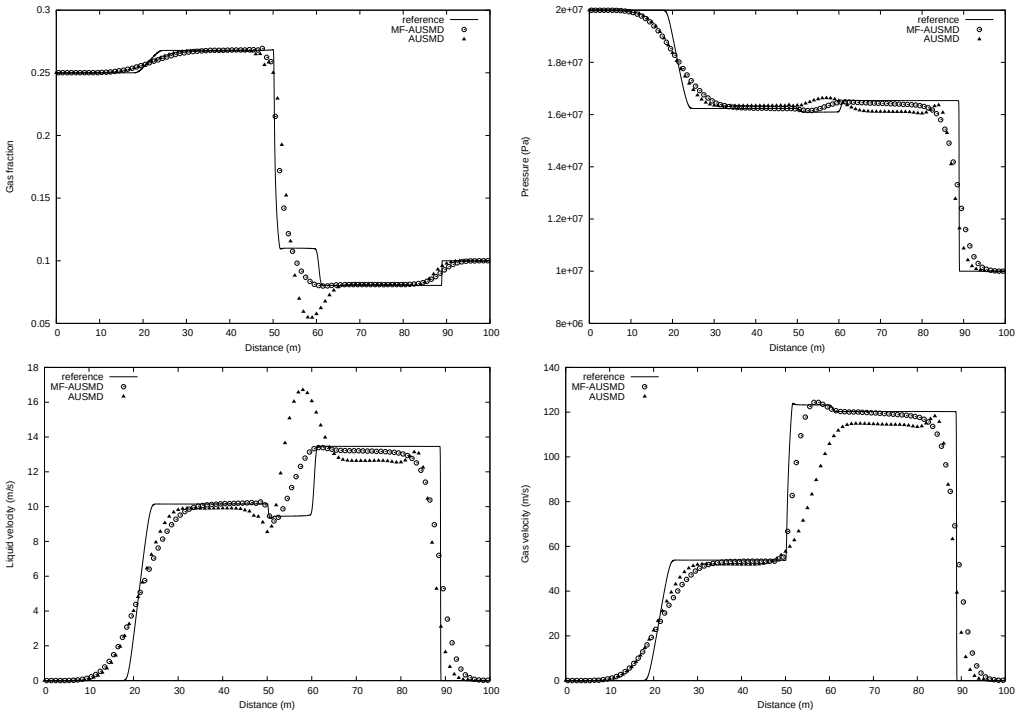

FIGURE 7. Toumi's shock tube problem, $T = 0.08$ s, 100 grid cells. MF-AUSMD vs basic AUSMD scheme. Top left: Gas fraction. Top right: Pressure. Bottom left: Liquid velocity: Bottom right: Gas velocity.

We note that the AUSMD scheme produces a large overshoot in the pressure variable, and is also inaccurate in the resolution of the left-moving sonic wave. MF-AUSMD is non-oscillatory, and produces here a solution that is intermediate between the Roe and AUSMD solution.

7.3. **Toumi's Water-Air Shock.** We now consider an initial value problem of a kind introduced by Toumi [27] and investigated by Tiselj and Petelin [26] and Paillère et al [17]. The initial states are given by

$$\mathbf{W}_{\mathrm{L}} = \begin{bmatrix} p \\ \alpha_{\mathrm{l}} \\ v_{\mathrm{g}} \\ v_{\mathrm{l}} \end{bmatrix} = \begin{bmatrix} 2 \cdot 10^7 \text{ Pa} \\ 0.75 \\ 0 \\ 0 \end{bmatrix} \tag{73}$$

and

$$\mathbf{W}_{\mathrm{R}} = \begin{bmatrix} p \\ \alpha_{\mathrm{l}} \\ v_{\mathrm{g}} \\ v_{\mathrm{l}} \end{bmatrix} = \begin{bmatrix} 1 \cdot 10^7 \text{ Pa} \\ 0.9 \\ 0 \\ 0 \end{bmatrix}. \tag{74}$$

Again no source terms are taken into account. Following Paillère et al [17], we modify the interfacial pressure correction (11) for this problem, setting $\sigma = 2$.

7.3.1. *Comparison between MF-AUSMD and basic AUSMD scheme.* Results after $T = 0.08$ s are given in Figure 7, using a grid of 100 cells and a timestep $\Delta x/\Delta t = 1000$ m/s. The reference solution was calculated by the MF-AUSMD scheme on a grid of 10 000 cells. We note that we achieve a wave structure that is highly similar to the one reported by Paillère et al [17], although slightly different submodels are used. This observation supports our belief that the wave structure of the model is largely unaffected by the inclusion of energy equations, as stated in Remark 1.

This example demonstrates overshoots for the basic AUSMD scheme whereas the MF-AUSMD scheme is fully nonoscillatory.

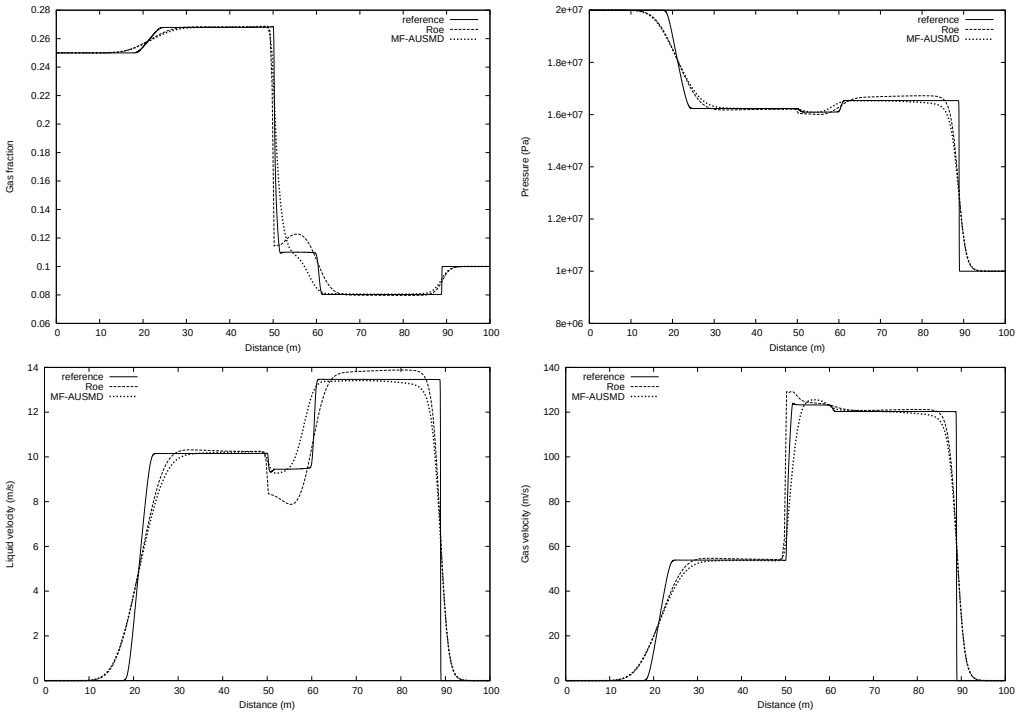

FIGURE 8. Toumi's shock tube problem, $T = 0.08$, 200 grid cells. MF-AUSMD vs Roe scheme. Top left: Gas fraction. Top right: Pressure. Bottom left: Liquid velocity: Bottom right: Gas velocity.

7.3.2. *Comparison between MF-AUSMD and Roe scheme.* Results after $T = 0.08$ s are given in Figure 8, using a grid of 200 cells and a timestep $\Delta x/\Delta t = 1000$ m/s.

We observe that the Roe and MF-AUSMD schemes give a similar resolution of the sonic waves for this problem. However, tendencies for overshoots on the volume fraction waves are observed for the Roe scheme whereas the the MF-AUSMD scheme is nonoscillatory. On the other hand, MF-AUSMD seems more diffusive on the near-stationary discontinuity at $x = 50$ m.

7.3.3. *Convergence properties of the MF-AUSMD scheme.* In Figure 9 we study the convergence of the MF-AUSMD scheme as the grid is refined. The result demonstrates that the MF-AUSMD approaches the reference solution without introducing any spurious oscillations.

7.4. **Water Faucet Problem.** We now wish to focus more on the resolution of volume fraction waves. For this purpose we revisit the water faucet problem studied in Section 4.2.

7.4.1. *Comparison between MF-AUSMD and Roe scheme.* In Figure 10 the MF-AUSMD is compared to the Roe scheme for $T = 0.6$ s on a grid of 120 computational cells. The timestep $\Delta x/\Delta t = 10^3$ m/s is used. The pressure reference was calculated using MF-AUSMD on a grid of 12 000 cells, for gas fraction and liquid velocity the approximate analytical expressions were used. Only for the pressure does the plot demonstrate any notable difference between the schemes - the MF-AUSMD is somewhat more diffusive than the Roe scheme.

7.4.2. *Convergence properties of the MF-AUSMD scheme.* In Figure 11 we investigate how the scheme converges to the expected analytical solution as the grid is refined. In Section 4.2 we found that AUSMD produces small overshoots in the volume fraction for very fine grids. A similar behaviour was reported by Paillére et al [17] for their AUSM$^+$ scheme. As we can see, no overshoots are produced by the MF-AUSMD scheme, and by that the improved approximation properties of the MF-AUSMD scheme over the AUSMD scheme are verified.

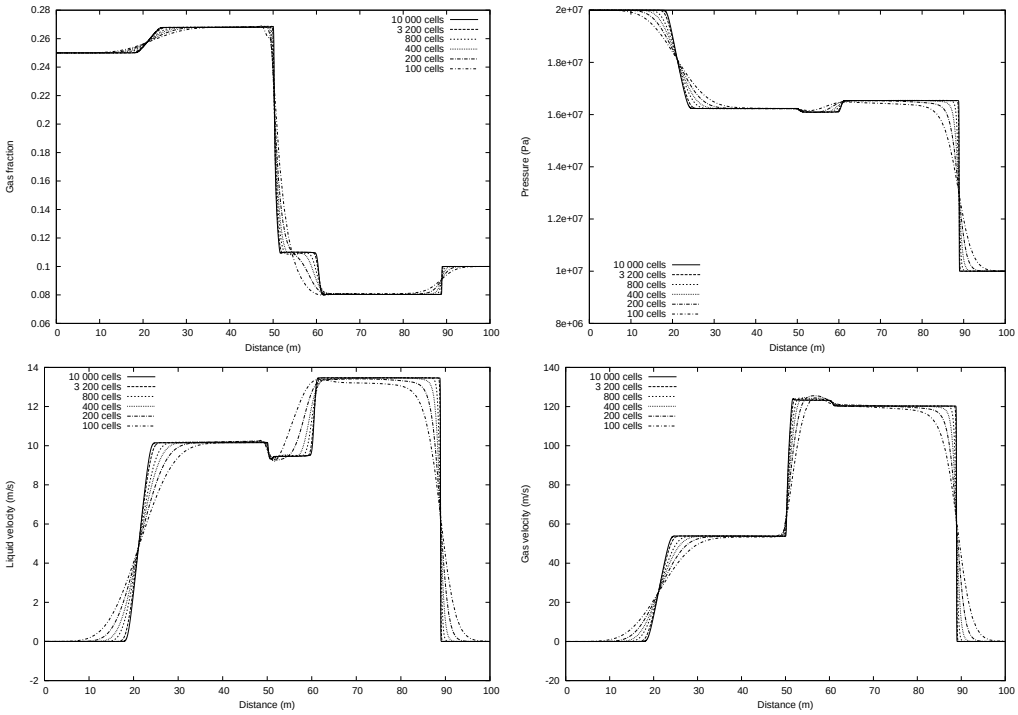

FIGURE 9. Toumi's shock tube problem. Grid refinement for the MF-AUSMD scheme. Top left: Gas fraction. Top right: Pressure. Bottom left: Liquid velocity: Bottom right: Gas velocity.

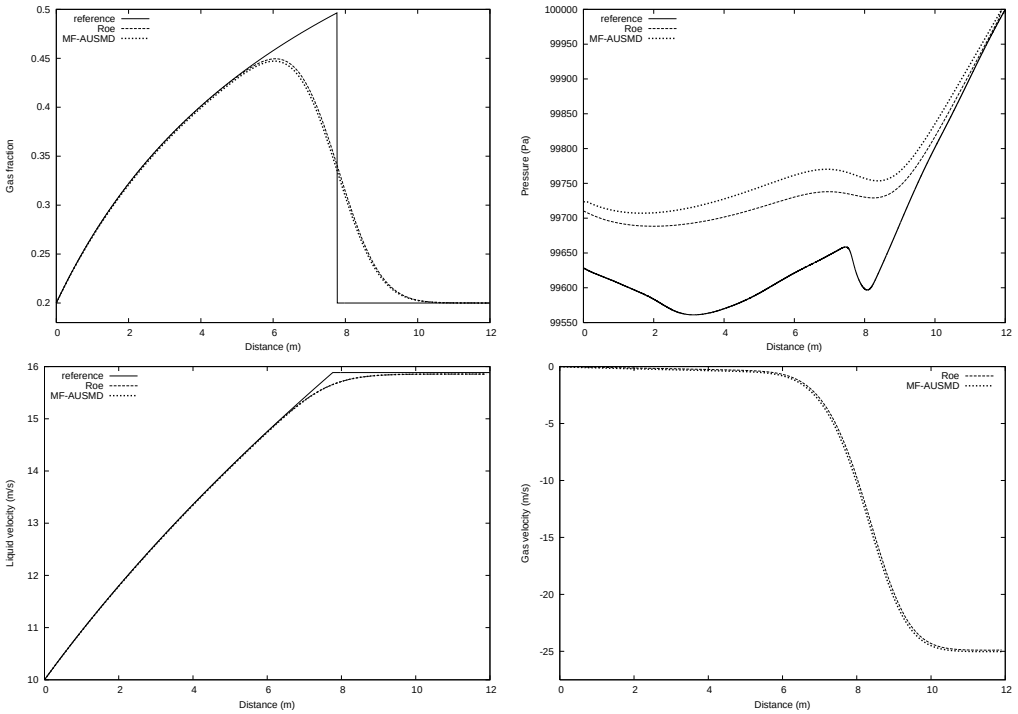

FIGURE 10. Water faucet problem, $T = 0.6$ s, 120 grid cells. MF-AUSMD vs Roe scheme. Top left: Gas fraction. Top right: Pressure. Bottom left: Liquid velocity: Bottom right: Gas velocity.

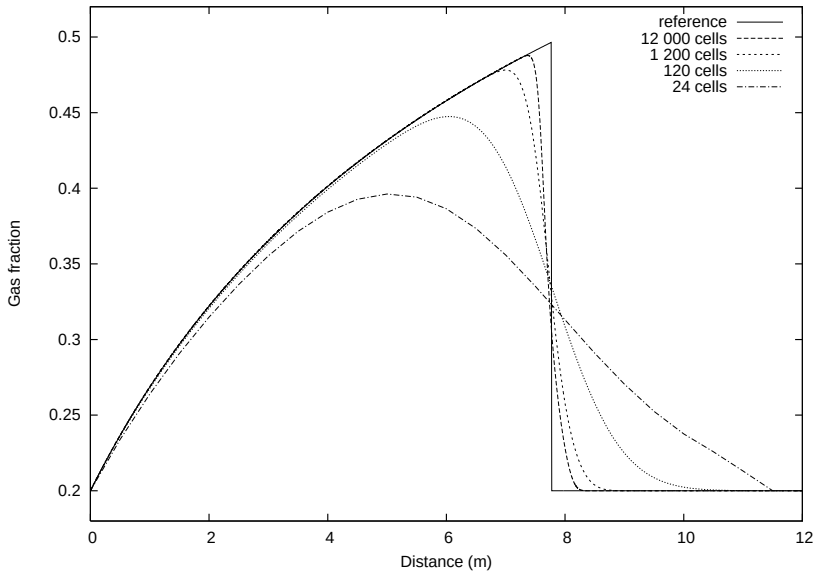

FIGURE 11. Water faucet problem, T=0.6 s. Convergence properties of the MF-AUSMD scheme.

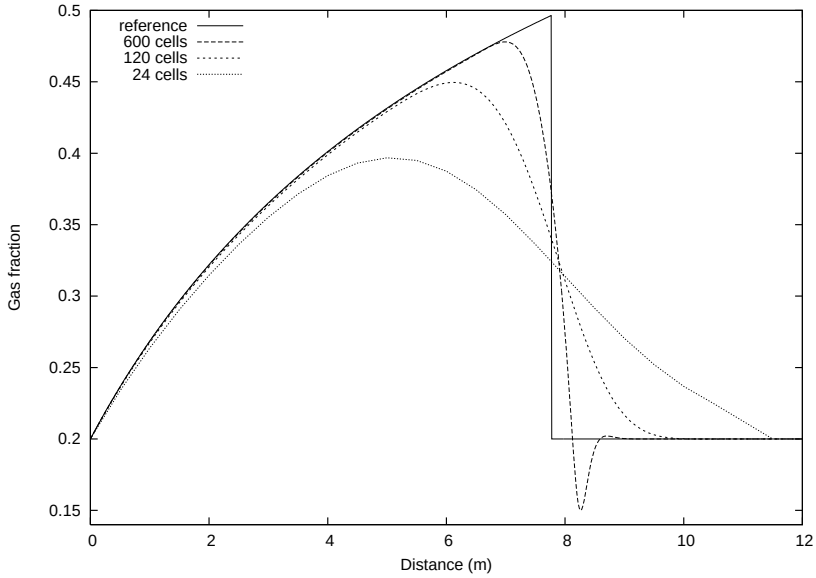

FIGURE 12. Water faucet problem, T=0.6s. Non-hyperbolic model. Convergence properties of the MF-AUSMD scheme.

7.4.3. *Non-hyperbolic model.* We now consider a non-hyperbolic model, that is in the framework of (11) we consider the choice

$$\sigma = 0. \tag{75}$$

Paillère et al [17] found that for this non-hyperbolic model, oscillations were produced near the discontinuity as the grid was refined. We now want to investigate to which degree this effect is independent of the numerical scheme, and to which degree the dissipative mechanism of different schemes act differently in magnifying the expected oscillatory behaviour of a non-hyperbolic model. The effect of grid refinement for the MF-AUSMD scheme is demonstrated in Figure 12.

We observe that an oscillation is produced to the right of the discontinuity for the grid of 600 cells. In fact it was observed that for 1200 cells, this oscillation would grow to the point were the scheme exploded. This confirms the assertion of Paillère et al [17] that we should expect oscillations of a mathematical nature for this test case, demonstrating the importance of using a hyperbolic model.

7.5. **Separation Problem.** We now consider the separation problem introduced by Coquel et al [3], previously investigated by Evje and Flatten [9] and Paillère et al [17]. We consider a vertical pipe of length 7.5 m, where gravitational acceleration is the only source term taken into account. Initially the pipe is filled with stagnant liquid and gas with a uniform pressure of $p_0 = 10^5$ Pa and a uniform liquid fraction of $\alpha_{\rm l} = 0.5$. The pipe is considered to be closed at both ends, i.e. both phasic velocities are forced to be zero at the end points.

The following approximate analytical solution was presented in [9]

$$v_{\rm l}(x,t) = \begin{cases} \sqrt{2gx} & \text{for } x < \frac{1}{2}gt^2 \\ gt & \text{for } \frac{1}{2}gt^2 \leq x < L - \frac{1}{2}gt^2 \\ 0 & \text{for } L - \frac{1}{2}gt^2 < x \end{cases} \tag{76}$$

$$\alpha_{\rm l}(x,t) = \begin{cases} 0 & \text{for } x < \frac{1}{2}gt^2 \\ 0.5 & \text{for } \frac{1}{2}gt^2 \leq x < L - \frac{1}{2}gt^2 \\ 1 & \text{for } L - \frac{1}{2}gt^2 < x \end{cases} \tag{77}$$

where $L = 7.5$ m is the length of the tube. This approximate solution consists of a contact discontinuity at the top of the tube and a shock-like discontinuity at the lower part of the tube. After the time

$$T = \sqrt{\frac{L}{g}} = 0.87 \text{ s} \tag{78}$$

these discontinuities will merge and the phases become fully separated. The volume fraction reaches a stationary state, whereas the other variables slowly converge towards a stationary solution. In particular we expect the stationary pressure to be fully hydrostatic, approximately given by

$$p(x,t) = \begin{cases} p_0 & \text{for } x < L/2 \\ p_0 + \rho_{\rm l} g\,(x - L/2) & \text{for } x \geq L/2. \end{cases} \tag{79}$$

7.5.1. *Transition to One-Phase Flow.* We observed that the basic MF-AUSMD scheme would produce instabilities in the transition to one-phase flow. Indeed this is a common problem for two-phase flow models, observed among others by Coquel et al [3] for their kinetic scheme, Paillére et al [17] for their AUSM$^+$ scheme and Romate [21] for his Roe scheme. Romate suggested a scheme switching strategy for solving this problem, where the original scheme is replaced with a stable, diffusive scheme near one-phase regions.

In [9] we introduced a modification of the basic AUSMD scheme, denoted as AUSMDV*, where we took advantage of a highly robust flux vector splitting (FVS) scheme to achieve a stable transition to one-phase flow. Using a frictionless model, we observed strong velocity gradients for the disappearing phase. Such large velocities are unphysical and may also cause the pressure variable to fail to converge to a hydrostatic distribution [9].

In this paper we follow the approach of Paillére et al [17], and include an interface momentum exchange term on the form

$$M_{\rm g}^{\rm D} = C\alpha_{\rm g}\alpha_{\rm l}\rho_{\rm g}(v_{\rm g} - v_{\rm l}), \tag{80}$$

where $C > 0$ and $M_{\rm l}^{\rm D} = -M_{\rm g}^{\rm D}$, conserving total momentum.

In addition to allowing for more physically valid velocity calculations, this term also prevents numerical instabilities related to large relative velocities in the one-phase regions. This allows for a stable numerical transition to one-phase flow using only a slight modification of the MF-AUSMD scheme, as described in the following.

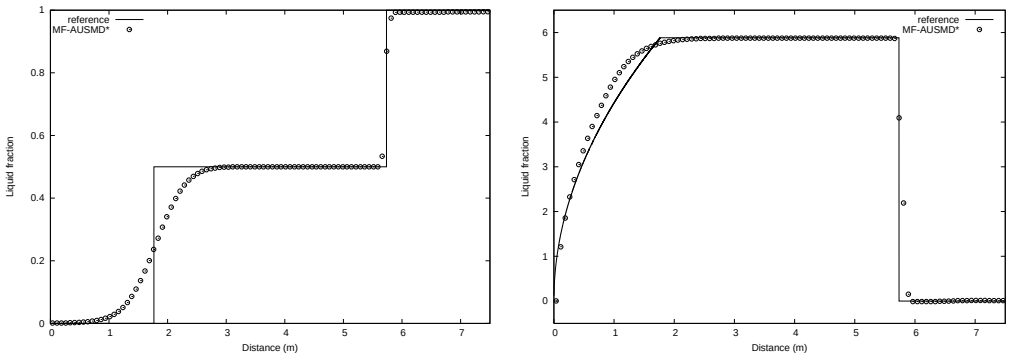

FIGURE 13. Separation problem, T=0.6 s. MF-AUSMD* scheme, 100 cells. Left: Liquid fraction. Right: Liquid velocity.

Definition 2. *We consider a hybrid of the MF-AUSMD and the van Leer scheme, denoted as* **MF-AUSMD***, *where the numerical mass fluxes are given by the following expression*

$$\mathbf{F}^{\mathrm{MF-AUSMD}^*} = s\mathbf{F}^{\text{van Leer}} + (1-s)\mathbf{F}^{\mathrm{MF-AUSMD}}. \tag{81}$$

Here s is chosen as

$$s = \max(\phi_{\mathrm{L}}, \phi_{\mathrm{R}}), \tag{82}$$

where ϕ is an indicator function designed to be 1 near one-phase regions, 0 otherwise.

For the purposes of this paper we choose

$$\phi_j = e^{-k[\alpha_{\mathrm{g}}]_j^n} \tag{83}$$

where we use the parameter $k = 50$.

We note that the MF-AUSMD* scheme differs from the MF-AUSMD scheme only near one-phase liquid regions. For the coefficient C of (80), we choose the expression

$$C = C_0\phi_j, \tag{84}$$

ensuring that the interface friction acts more strongly near one-phase liquid regions where we expect the gas to dissolve in the liquid. For the value C_0 we follow Paillére et al [17] and choose

$$C_0 = 50000 \text{ s}^{-1}. \tag{85}$$

7.5.2. *Numerical results.* Results after $T = 0.6$ s are plotted in Figure 13, using a grid of 100 cells and a timestep $\Delta x/\Delta t = 2000$ m/s. We note that good accordance with the expected analytical solution is achieved.

Results after $T = 1.5$ s are plotted in Figure 14, using the same grid. Now fully stationary conditions are reached. Again we observe good agreement with the approximate analytical solutions.

7.5.3. *Convergence properties of the MF-AUSMD* scheme.* In Figure 15 the effect of grid refinement on resolution of volume fraction is illustrated for the MF-AUSMD* scheme at the time of T=0.6 s. The figure indicates that the expected analytical solution is approached in a monotone way.

8. SUMMARY

We have presented a framework, the Mixture Flux (MF) method, for constructing accurate and robust numerical schemes for the two-fluid model. The framework may be viewed as a refinement of previously studied flux-splitting schemes, involving a stronger coupling between the phasic variables in accordance with the mixture nature of the model. Particularly, we have constructed a numerical scheme on the basis of the AUSMD flux used in [9], demonstrating that we keep the accuracy properties of the basic AUSMD while significantly improving its stability properties. In particular we have demonstrated that the resulting MF-AUSMD scheme compares very well

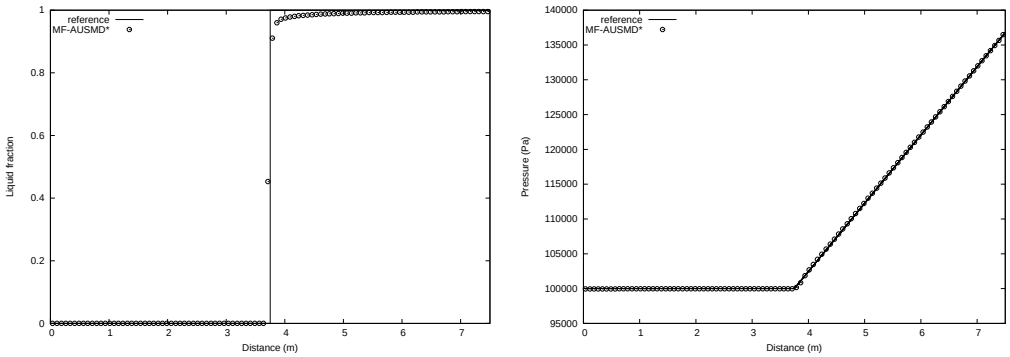

FIGURE 14. Separation problem, T=1.5 s. MF-AUSMD* scheme, 100 cells. Top left: Liquid fraction. Top right: Pressure. Bottom left: Liquid velocity. Bottom right: Gas velocity.

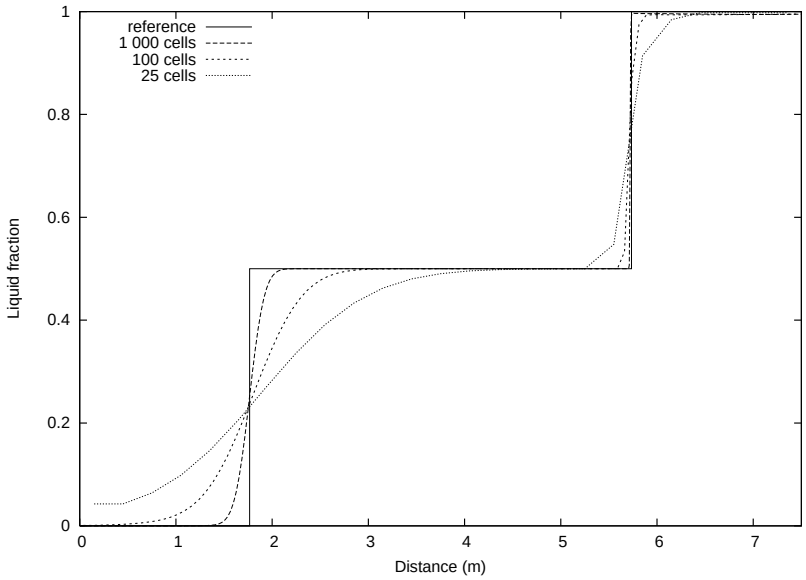

FIGURE 15. Separation problem, T=0.6s. Convergence properties of the MF-AUSMD* scheme.

with the Roe scheme in terms of accuracy and robustness for several different test cases. Most importantly the MF-AUSMD does not involve solving a local Riemann problem by eigenstructure decomposition and is therefore superior to the Roe scheme when it comes to computational efficiency.

Acknowledgements. The first author thanks the Norwegian Research Council for financial support through the "Petronics" programme.

REFERENCES

[1] R. Abgrall, How to prevent pressure oscillations in multicomponent flow calculations, *J. Comput. Phys.* **125**, 150–160, 1996.

[2] K. H. Bendiksen, D. Malnes, R. Moe, and S. Nuland, The dynamic two-fluid model OLGA: Theory and application, in *SPE Prod. Eng.* **6**, 171–180, 1991.

[3] F.Coquel, K. El Amine, E. Godlewski, B. Perthame, and P. Rascle, A numerical method using upwind schemes for the resolution of two-phase flows, *J. Comput. Phys.* **136**, 272–288, 1997.

[4] J. Cortes, A. Debussche, and I. Toumi, A density perturbation method to study the eigenstructure of two-phase flow equation systems, *J. Comput. Phys.* **147**, 463–484, 1998.
[5] J. R. Edwards and M.-S. Liou, Low-diffusion flux-splitting methods for flows at all speeds, *AIAA Journal* **36**, 1610-1617, 1998.
[6] J. R. Edwards, R. K. Franklin, and M.-S. Liou, Low-diffusion flux-splitting methods for real fluid flows with phase transition, *AIAA Journal* **38**, 1624-1633, 2000.
[7] S. Evje and K. K. Fjelde, Hybrid flux-splitting schemes for a two-phase flow model, *J. Comput. Phys.* **175**, 674–701, 2002.
[8] S. Evje and K. K. Fjelde, On a rough ausm scheme for a one-dimensional two-phase flow model, *Comput. & Fluids* **32**, 1497–1530, 2003.
[9] S. Evje and T. Flatten. Hybrid flux-splitting schemes for a common two-fluid model. *J. Comput. Phys*, to appear.
[10] K.-K. Fjelde and K.H. Karlsen, High-resolution hybrid primitive-conservative upwind schemes for the drift flux model, *Comput. & Fluids* **31**, 335–367, 2002.
[11] A. Harten, P.D. Lax and B. Van Leer, On upstream differencing and Godunov schemes for hyperbolic conservation laws, *SIAM Review.* **25**, 35–61, 1981.
[12] M.-S. Liou, A sequel to AUSM: AUSM(+), *J. Comput. Phys.* **129**, 364–382, 1996.
[13] M.-S. Liou and C. J. Steffen, A new flux splitting scheme, *J. Comput. Phys.* **107**, 23-39, 1993.
[14] Y. Y. Niu, Simple conservative flux splitting for multi-component flow calculations, *Num. Heat Trans.* **38**, 203-222, 2000.
[15] Y.-Y. Niu, Advection upwinding splitting method to solve a compressible two-fluid model, *Int. J. Numer. Meth. Fluids* **36**, 351–371, 2001.
[16] S. Osher, Riemann solvers, the entropy conditions, and difference approximations, *SIAM J. Num. Anal.* **21**, 217–235, 1984.
[17] H. Paillère, C. Corre and J.R.G Cascales, On the extension of the AUSM+ scheme to compressible two-fluid models, *Comput. & Fluids* **32**, 891–916, 2003.
[18] V. H. Ransom, Numerical bencmark tests, *Multiphase Sci. Tech.* **3**, 465-473, 1987.
[19] P.L. Roe, The use of Riemann problem in finite difference schemes, *Lectures Notes of Physics* **141**, 354–359, 1980.
[20] P.L. Roe. Approximate Riemann solvers, parameters vectors and difference schemes, *J. Comput. Phys.* **43**, 357–372, 1981.
[21] J. E. Romate, An approximate riemann solver for a two-phase flow model with numerically given slip relation, *Comput. & Fluids* **27**, 455–477, 1998.
[22] R. Saurel and R. Abgrall, A multiphase godunov method for compressible multifluid and multiphase flows, *J. Comput. Phys.* **150**, 425–467, 1999.
[23] R. Saurel and R. Abgrall. A simple method for compressible multifluid flows. *SIAM J. Sci. Comput.* **21**, 1115–1145, 1999.
[24] H. B. Stewart and B. Wendroff, Review article; two-phase flow : Models and methods, *J. Comput. Phys.* **56**, 363–409, 1984.
[25] E. Tadmor. Numerical viscosity and the entropy condition for conservative difference schemes. *Mathematics of Computation.* **43**, 369–381, 1984.
[26] I. Tiselj and S. Petelin, Modelling of two-phase flow with second-order accurate scheme, *J. Comput. Phys.* **136**, 503–521, 1997.
[27] I. Toumi, An upwind numerical method for two-fluid two-phase flow models, *Nuc. Sci. Eng.* **123**, 147–168, 1996.
[28] I. Toumi and A. Kumbaro, An approximate linearized riemann solver for a two-fluid model, *J. Comput. Phys.* **124**, 286–300, 1996.
[29] J. A. Trapp and R. A. Riemke, A nearly-implicit hydrodynamic numerical scheme for two-phase flows, *J. Comput. Phys.* **66**, 62–82, 1986.
[30] Y. Wada and M.-S. Liou, An accurate and robust flux splitting scheme for shock and contact discontinuities, *SIAM J. Sci. Comput.* **18**, 633–657, 1997.